

Molecular compositions and optical properties of dissolved brown carbon in biomass burning, coal combustion, vehicle emission aerosols illuminated by excitation-emission matrix spectroscopy and FT-ICR MS analysis

Jiao Tang^{1,4}, Jun Li^{*,1}, Tao Su^{1,4}, Yong Han², Yangzhi Mo¹, Hongxing, Jiang^{1,4}, Min Cui², Bin Jiang¹, Yingjun Chen², Jianhui Tang³, Jianzhong Song¹, Ping'an Peng¹, Gan Zhang^{*,1}

¹State Key Laboratory of Organic Geochemistry, Guangzhou Institute of Geochemistry, Chinese Academy of Sciences, Guangzhou 510640, China

²Department of Environmental Science and Engineering, Fudan University, Shanghai 200092, P.R. China

³Key Laboratory of Coastal Environmental Processes and Ecological Remediation, Yantai Institute of Coastal Zone Research, Chinese Academy of Sciences, Yantai 264003, China

⁴University of Chinese Academy of Sciences, Beijing 100049, China

***Corresponding authors:** Jun Li (junli@gig.ac.cn); Gan Zhang (zhanggan@gig.ac.cn)

Abstract: Brown carbon (BrC) plays an essential impact on radiative forcing due to its ability to absorb sunlight. In this study, the optical properties and molecular characteristics of water-soluble and methanol-soluble organic carbon (MSOC) emitted from the simulated combustion of biomass and coal fuels, and vehicle emissions were investigating using UV-visible spectroscopy, excitation-emission matrix (EEM) spectroscopy, and Fourier-transform ion cyclotron resonance mass spectrometry (FT-ICR MS) coupled with electrospray ionization (ESI). The results showed that these smoke aerosols of biomass burning (BB) and coal combustion (CC) had a higher mass absorption efficiency at 365 nm (MAE_{365}) than that of vehicle emissions. A stronger MAE_{365} value was also found in MSOC than water-soluble organic carbon (WSOC), indicating low polar compounds would possess higher light absorption capacity. Parallel factor analysis (PARAFAC) identified six types of fluorophores in the WSOC including two humic-like substances (HULIS-1) (P1, and P6), three protein-like substances (PLOM) (P2, P3, and P5), and one undefined (P4). HULIS-1 was mainly from aging vehicle exhausts, P2 was only abundant in BB aerosols, P3 was ubiquitous in all tested aerosols, P4 was abundant in fossil burning aerosols, and P5 was more intense in the fresh vehicle-exhaust particles. The MSOC chromophores (six components, C1-C6) exhibited consistent characteristic with WSOC, suggesting the method could be used to indicate the origins of chromophores. FI-ICR mass spectra showed that CHO and CHON were the most abundant components of WSOC, but S-containing compounds appeared a higher abundance in the CC aerosols and vehicle emission than BB aerosols. While, considerably low S-containing compounds with largely CHO and CHON were detected in MSOC. The unique formulas of different sources determined by the Venn diagram presented different molecular distribution. To be specific, BB aerosols with largely CHO and CHON had a medium H/C and low O/C ratio; while, CC aerosols and vehicle emissions with largely S-containing compounds had an opposite H/C and O/C ratio. Moreover, the light absorption capacity of WSOC and MSOC was positively associated with the unsaturation degree and molecular weight in the source aerosols. The above results are potentially applicable to further studies on EEM-based or

48 molecular characteristic-based source apportionment of chromophores in atmospheric
49 aerosols.
50

1 Introduction

Carbonaceous aerosols play an important role in the Earth's radiative balance. One such aerosol, black carbon (BC), absorbs significant amounts of light and exerts a warming effect, while organic carbon (OC) was initially thought to only scatter solar radiation (Wong et al., 2017; Mo et al., 2017; Saleh et al., 2014). However, recent studies show that there are certain types of OC absorb radiation efficiently in the near-ultraviolet (UV) (300–400 nm) and visible ranges, which are called brown carbon (BrC). They can positively shift the net direct radiation forcing (DRF) (Saleh et al., 2014; Laskin et al., 2015; Kirchstetter and Thatcher, 2012). According to a simulation model, the inclusion of BrC may enhance total aerosol absorption by 7–19% (Feng et al., 2013). According to previous study, BrC in atmospheric aerosols mainly originates from emissions from biomass burning (BB) and coal combustion (CC), vehicle exhausts, and the formation of secondary organic aerosol (SOA) (Zhu et al., 2018; Laskin et al., 2015; Xie et al., 2017; Kumar et al., 2018). Among them, primary emissions contributed significantly to BrC absorption (Fan et al., 2012; Yan et al., 2015; Zhang et al., 2011). Recently, many studies have investigated the optical properties and molecular characteristic of BrC in laboratory simulated combustion (Budisulistiorini et al., 2017; Lin et al., 2018; Lin et al., 2016; Song et al., 2019) and their light absorption in controlled vehicle emissions (Xie et al., 2017). However, there were no available studies on the comprehensive characteristic of BrC in various sources and their variations in optical and chemical information impacted by these sources, therefore, investigating the BrC in different sources would improve our understanding of the evolution of BrC absorption.

Excitation-emission matrix (EEM) spectroscopy can provide structure information of chromophores and thus has been widely applied to identify the sources and chemical nature of chromophoric dissolved organic matter (CDOM) in aquatic environments since the 1990s (Shimabuku et al., 2017; Wells et al., 2017; Bhattacharya and Osburn, 2017; Coble, 1996). Due to the optical properties of chromophoric water-soluble organic carbon (WSOC) in the atmosphere were similar to CDOM in aquatic environments (Qin et al., 2018; Fu et al., 2015; Graber and Rudich, 2006), this

technique could extend to atmospheric research. It has to be mentioned that fluorescence is a radiative process that occurs between two energy levels of the same multiplicity (Andrade-Eiroa et al., 2013). Generally, compounds with rigid planar structures and highly conjugated systems have intrinsic fluorescence emission characteristics and are important BrC chromophores, such as aromatic acids, phenols, nitroaromatics, polycyclic aromatic hydrocarbons (PAHs), quinones, and so on (Lin et al., 2018; Zhang et al., 2013). Therefore, chromophores in fluorescence spectra could be considered as a “fingerprinting” tool, especially when combining it with parallel factor (PARAFAC) analysis which can decompose EEMs signal into their underlying chemical components (Murphy et al., 2013). For instance, Chen et al., (2016b) observed that the water-extracted chromophores identified by PARAFAC from the urban, forest, and marine aerosols were varied with the sampling sites and periods, and were affected by oxidative and functional groups. Lee et al., (2013) illustrated that SOA derived from the oxidation of limonene and decene with O₃ and OH had different fluorescence spectra. Therefore, BrC characteristics from various sources may differ. When analyzing chromophoric BrC using fluorescence spectra, however, is the lack of a classification system for fluorescence spectra, to distinguish chromophores from most non-absorbing constituents and to determine the chemical structures of the chromophores.

Fourier-transform ion cyclotron resonance mass spectrometry (FT-ICR MS) coupled with electrospray ionization (ESI) is a powerful platform for the detailed characteristics investigation of organic material at the molecular level. With the advantage of ultrahigh-resolution, the accuracy of mass measurements, and high sensitivity (Feng et al., 2016), FT-ICR MS has been successfully used to characterize organic aerosol (Jiang et al., 2016; Song et al., 2018; Mo et al., 2018), cloud water (Zhao et al., 2013), and natural organic matter (Sleighter et al., 2012; Feng et al., 2016). For example, a relative study has determined their molecular families of dissolved organic matters (DOMs) associated with fluorescent components by using FI-ICR MS (Stubbins et al., 2014), which could provide more chemical information of chromophores.

Residential CC and BB emissions, and motor vehicle emissions are significant anthropogenic sources of air pollutants, exceptionally fine particulate matter (PM_{2.5}) on urban and regional scales (Gentner et al., 2017; Yan et al., 2015; Zhang et al., 2018; Chen et al., 2015). In this study, to obtain a comprehensive understanding of BrC originating from various sources, UV-vis, EEMs, and FI-ICR MS analysis were performed for water-soluble and methanol-soluble organic carbon (MSOC) from the smoke particles of simulated combustion of biomass fuels and coals, and vehicle emission aerosols. Statistical analysis of PARAFAC was applied to EEM spectra to resolve the fluorescent compounds. All, and unique molecular characteristic of water-soluble organic carbon (WSOC) and MSOC were analyzed and discussed on the base of FI-ICR MS. Relationship between optical properties and chemical structures were discussed by using linear regression coefficient.

2 Experimental methods

2.1 Sample collection and preparation

The smoke particles were collected by the instrument coupled with a dilution channel which was designed to simulate fire emissions representative of “real-world” open BB and household CC activities (Figure S1). In the present study, a total of 27 BB samples (IDs1-27) were collected at Xishuangbanna city, Yunnan Province, from May 20th to June 3th, 2016 and the detailed sampling process was described in our previous article (Cui et al., 2018). In short, raw fuels (rough 20×3×2 cm³) were air-dried for several days and ignited in a stainless-steel bowl, and then the rising smoke was collected through a dilution system. The sampling system mainly consisted of a dilution tunnel, a residence time chamber, three particulate matter (PM) samplers, and so on. Every biomass was burned three times, about 1-2 kg fuels per burn. Every combustion process lasted for 20 minutes. The collection of smoke particles started when the fuel ignited, and end until the concentration of CO₂ down to atmosphere CO₂ level. Dilution ratios of each experimental process were calculated using the CO₂ concentrations before and after dilution. The collection flow rate and

average dilution ratio were 180 L/min and 2.1, respectively. And the other 6 BB samples (IDs28-33) were collected in Guangzhou city, Guangdong Province.

The smoke particles of CC (IDs34-50) were collected as same as that of BB experiment, but used a stove, in Guangzhou city, Guangdong province, from Nov 18th, 2017 to Jan 23th, 2018. The tested stove is technically improved stoves (named Jin-Yin stove). Due to the difficulty of ignition of coal, we used smokeless charcoal to ignite one-third (about 300 g) of the raw-coal chunk (2-5 cm in size) in the stove, removed the charcoal after ignition, and then added the remaining raw-coal chunk (about 700 g) to start to collect the smoke particle. Every coal was also burned three times, about 1 kg fuels per burn. Every combustion process lasted for about 40-150 minutes. The collection flow rate and average dilution ratio were 150 L/min and 1.5, respectively. Additionally, modified combustion efficiency (MCE) was calculated to characterize the relative amount of smoldering and flaming combustion phase (Lin et al., 2016;Cui et al., 2018). The average MCE value was 0.73 ± 0.08 for CC experiment but unavailable for the BB experiment because the CO sensor did not work in the field work, which was mentioned in our previous paper (Cui et al., 2018).

Tunnel aerosols (total eight samples, IDs51-58) were collected at Siping Tunnel from Nov 1th to 2th, 2017 and Xiaoyangshan Tunnel from Dec 1th to 2th, 2017, in Shanghai city, as well as two vehicle exhaust particles (IDs59-60) were collected from the direct emission of two different trucks (more fresh aerosols). With no other instructions, vehicle emissions represented all tunnel aerosols and vehicle exhaust particles. These filters were wrapped in aluminum foil and pre-baked at 450 °C for 5 hours before sampling and stored at -20 °C after sampling. Overall, there was a total of 60 total suspended particulate matter (TSP) samples on source emissions in this study, and blank samples that were collected at different times and locations were used for correcting filter samples.

WSOC for UV-Vis absorption and EEM analysis was extracted with purified water (resistivity of $>18.2\Omega$) via ultra-sonication of quartz filter punches for 30 minutes. Because water cannot effectively extract the BrC (Liu et al., 2013;Shetty et al., 2019), the remaining filter was further freeze-dried and extracted with methanol

(HPLC grade) to obtain the MSOC constituent for better understand the optical properties and molecular composition of BrC. It is worth noting that the MSOC in this study is not necessarily like those of the same names in other studies. All the extracts were filtered through a 0.22 μm polytetrafluoroethylene membrane into amber colored glass vials to remove the insoluble material.

2.2 Carbon analysis

We measured both OC and elemental carbon (EC) using an aerosol carbon analyzer (Sunset Laboratory, Inc., USA), following the NIOSH thermal-optical transmittance (TOT) standard method (Mo et al., 2017), and the emission factors (EFs) of PM, OC and EC were calculated and detail information was presented in supplement. We also analyzed the elemental compositions of biomass (C, H, O, and N) and coal (C, H, O, N, and S) using an elemental analyzer (Vario EL cube; Elementar, Germany) and the results were listed in Table S1 and S2. The carbon content of WSOC was measured using total organic carbon analysis (Vario TOC cube; Elementar) before acidifying with phosphoric acid to remove inorganic carbon, while that of the MSOC was assessed using the method developed by a previous study (Chen et al., 2017b). In short, the extracted MSOC was dried gently under nitrogen, and then re-dissolved in 500 μL methanol. Subsequently, 50 μL of the solution was added to the clear quartz filter (area: 1.5 cm^2) until dry and analyzed using the TOT standard method.

2.3 UV–Vis absorption spectra and EEM fluorescence spectra

The UV-vis absorption and EEM spectra of WSOC and MSOC were analyzed using a UV-Vis spectrophotometer (UV-4802; Unico, China) and an Aqualog fluorometer (Horiba Scientific, USA), respectively. The wavelengths used to characterize the UV-vis spectra were between 200 to 800 nm at a step size of 2 nm. Purified water was used as a baseline correction before measure. Mass absorption efficiency (MAE, $\text{m}^2 \text{g}^{-1} \text{C}$) was obtained as the following equation (Li et al., 2018):

$$\text{MAE}_\lambda = A_\lambda \cdot \ln(10) / (C \cdot L) \quad (1)$$

Here, A_λ is the value of light absorption at the given wavelength given by the spectrophotometer; C ($\mu\text{g C mL}^{-1}$) is the concentration of WSOC and MSOC; L is the optical path length. Moreover, the pH of WSOC was measured for all samples within the range of 5.5-6.5, generally thought it did not affect the absorbance according to prior study (Chen et al., 2016a).

The emission and excitation wavelengths of the fluorescence spectra were from 245 to 580 nm and 240 to 500 nm, respectively. The wavelength increments of the emission and excitation scans were 4.66 and 3 nm, respectively. Further, we subtracted the contributions of the solvents to the fluorescence spectra.

2.4 Ultrahigh-resolution ESI FT-ICR MS analysis

The WSOC and MSOC of six selected samples including two BB aerosols (Musa and Hevea), two CC aerosols (a anthracite and bituminous coal), one day of tunnel aerosol (combined the aerosols in inlet and outlet of the tunnel in the same day, TA), and one vehicle exhaust particles were analyzed using FT-ICR MS. To remove inorganic ions before instrumental analysis, WSOC was further adjusted to pH = 2 by the addition of hydrochloric acid (HCl) and then passed through a solid-phase extraction cartridge (Oasis HLB, 30 μm , 60 mg/cartridge; Waters Corporation, USA). The constituent retained on the SPE cartridge was eluted with methanol containing 2% ammonia (v/v). Eluted samples were evaporated until dry under a gentle nitrogen gas stream. The extracted solutions by methanol was evaporated under a gentle nitrogen gas stream for preparation.

We used the analysis method of FT-ICR MS described in detail in our previous study (Mo et al., 2018). Briefly, ultrahigh-resolution mass spectra were obtained using a solariX XR FT-ICR MS (Bruker Daltonics GmbH, Bremen, Germany) equipped with a 9.4-T superconducting magnet and an ESI ion source. The system was operated in negative ionization mode. The ion accumulation time was set to 0.6 s. The lower and upper mass limit was set to m/z 150 and 800 Da, respectively. The mass spectra were externally calibrated with arginine clusters using a linear calibration and then internally recalibrated with typical O_6S_1 class species peaks using quadratic

calibration in DataAnalysis ver. 4.4 software (Bruker Daltonics). A typical mass-resolving power >450 000 at m/z 319 with <0.2 ppm absolute mass error was achieved. The mass spectra of field blank filters were analyzed to detect possible contamination following the same procedures. More data processing was presented in S1 of the supplement.

2.5 PARAFAC analysis for EEM spectra

PARAFAC analysis with non-negativity constraints was used to explore the fluorescent components in dissolved BrC based on the method established by Murphy et al (Murphy et al., 2013;Andersson and Bro, 2000), which was performed using drEEM toolbox version 2.0 using a MATLAB software (<http://models.life.ku.dk/drEEM>). This method had been widely applied to the analysis of fluorescence spectra in aerosols (Chen et al., 2016b;Chen et al., 2016a;Matos et al., 2015;Wu et al., 2019). Absorbance measurements was used to correct the EEM for inner filter effects (IFE) according to the previous studies (Luciani et al., 2009;Gu and Kenny, 2009;Fu et al., 2015). The highest light absorbance in the calibrated wavelength range of WSOC and MSOC was not greater than 2 (mostly below 1 at 254 nm), which is appropriate for the inner filter corrections of the EEMs (Gu and Kenny, 2009;Murphy et al., 2013). Each EEM was normalized to the Raman peak area of purified water collected on the same day to correct fluorescence in Raman Units (RU) at excitation 350 nm and corrected for the dilution factor (Murphy et al., 2013;Murphy et al., 2010). Additionally, the signals of the first-order and second-order Rayleigh and Raman scattering in the EEM were removed by an interpolation method (Bahram et al., 2006). Repeated convergence of the model was examined based on the iteration of the minimum square principle. The exploration phases of 2- to 7-components PARAFAC models contained an evaluation of the shape of spectral loading, leverage analysis, an examination of the core consistency, residual analysis, and split-half analysis (Figure S2-S7). Six-component PARAFAC model was identified and successfully passed the split-half validation with the split style of “S₄C₆T₃” for the WSOC and MSOC in 60 samples, respectively.

3 Results and discussions

3.1 Emission Characteristics and Optical Properties of Extracts.

The PM, OC, and EC emission factors (EFs) of 27 biomass and 17 coal combustion experiments were summarized in Table S3. The relevant EFs of some of the biomass species were reported previously (Cui et al., 2018). In this experiment, the EFs of PM, OC, and EC from burning 27 types of biomass were $15 \pm 11 \text{ g kg}^{-1} \text{ fuel}$, $8.0 \pm 6.4 \text{ g kg}^{-1} \text{ fuel}$, and $7.7 \times 10^{-1} \pm 3.4 \times 10^{-1} \text{ g kg}^{-1} \text{ fuel}$, respectively. The EFs emitted from bituminous CC (PM = $9.1 \times 10^{-1} \pm 6.5 \times 10^{-1} \text{ g kg}^{-1} \text{ fuel}$, OC = $4.2 \times 10^{-1} \pm 3.3 \times 10^{-1} \text{ g kg}^{-1} \text{ fuel}$, EC = $9.4 \times 10^{-2} \pm 1.9 \times 10^{-1} \text{ g kg}^{-1} \text{ fuel}$) were much higher than those of anthracite combustion (PM = $1.5 \times 10^{-1} \pm 8.9 \times 10^{-2} \text{ g kg}^{-1} \text{ fuel}$, OC = $1.2 \times 10^{-2} \pm 4.5 \times 10^{-3} \text{ g kg}^{-1} \text{ fuel}$, EC = $1.6 \times 10^{-4} \pm 1.4 \times 10^{-4} \text{ g kg}^{-1} \text{ fuel}$) in the same stove. These differences could be attributed to the high volatile matter content of bituminous coal (Tian et al., 2017; Chen et al., 2005). Note that when the fire had been ignited using one-third of the material, and then the remaining part was added, the CC smoke was collected. Thus, the results of our study would be lower than the real values.

MAE can be used to characterize the efficiency of solar energy absorption, which is represented by the degree of conjugation and the amount of electron delocalization in molecules (Chen et al., 2016a). As shown in Figure 1 and Table S4, MAE at 365 nm (MAE₃₆₅) was significantly higher in the case of BB and CC aerosols than in vehicle emissions in this study, consistent with the previous findings (Xie et al., 2017; Fan et al., 2016). Bituminous CC aerosols had higher MAE₃₆₅ values than anthracite combustion aerosols. At there, we introduced the EC/OC ratios, which could be used as an indicator of fire conditions (Xie et al., 2017). Figure S8 showed the MAE₃₆₅ of WSOC vs. EC/OC relationships for all BB and CC aerosols. The data clearly showed that the light absorption of BB aerosols was dependent on the burn conditions. However, weak relationship ($p > 0.05$) in CC aerosols suggested another factor may influence the light absorption, such as maturity (Li et al., 2018). Compared to WSOC, higher MAE₃₆₅ values were observed in the MSOC collected from BB ($2.3 \pm 1.1 \text{ m}^2 \text{ g}^{-1} \text{C}$) and bituminous CC ($3.2 \pm 1.1 \text{ m}^2 \text{ g}^{-1} \text{C}$) aerosols. This could be due to

the fact that these strongly light-absorbing fat-soluble components are likely to be large molecular weight PAHs, and quinones from BB and fossil fuel combustion (Sun et al., 2007; Chen and Bond, 2010), which were more soluble in low polar solution, but we obtained the opposite results in the case of anthracite combustion and vehicle emissions.

The MAE₃₆₅ of WSOC in this study was compared with the other studies (Figure 1). The BB aerosols in this study had a higher MAE₃₆₅ value than those in controlled BB experiments, while it was comparable to corn straw burning emissions (Park and Yu, 2016; Fan et al., 2016). Besides, the simulated BB aerosols exhibited higher MAE₃₆₅ values than those in highly BB-impacted areas (Hecobian et al., 2010), indicating the aging in the transport process could reduce the light absorption (Dasari et al., 2019). The CC aerosols showed a higher MAE₃₆₅ value than the other coal experiment (Li et al., 2018; Fan et al., 2016), while a comparable value to water-soluble BrC was observed in winter of Beijing (Cheng et al., 2011; Yan et al., 2015). The result indicated the strong influence of BrC in this season in this region. Besides, the simulated combustion aerosols in this study exhibited higher MAE₃₆₅ values than the other areas (such as Guangzhou, Nanjing, Los Angeles, Korea, Nepal, and so on) (see Figure 1).

Methanol has a lower polarity than water and can extract the water-insoluble compounds that are generally stronger chromophores. Chen et al., (2017b) extracted organic matters in aerosols using different polar solutions, and they found water-insoluble organic matters (WIOM) had a higher MAE value than the water-soluble organic matters (WSOM), consistent with our result in the BB and bituminous CC aerosols. Vehicle emission aerosols generally had a lower MAE value such as methanol-soluble BrC ($0.62 \pm 0.76 \text{ m}^2 \text{ g}^{-1}\text{C}$) in controlled emission experiment (Xie et al., 2017), which was comparable to WSOC ($0.71 \pm 0.30 \text{ m}^2 \text{ g}^{-1}\text{C}$) but higher than MSOC ($0.26 \pm 0.09 \text{ m}^2 \text{ g}^{-1}\text{C}$) in this study.

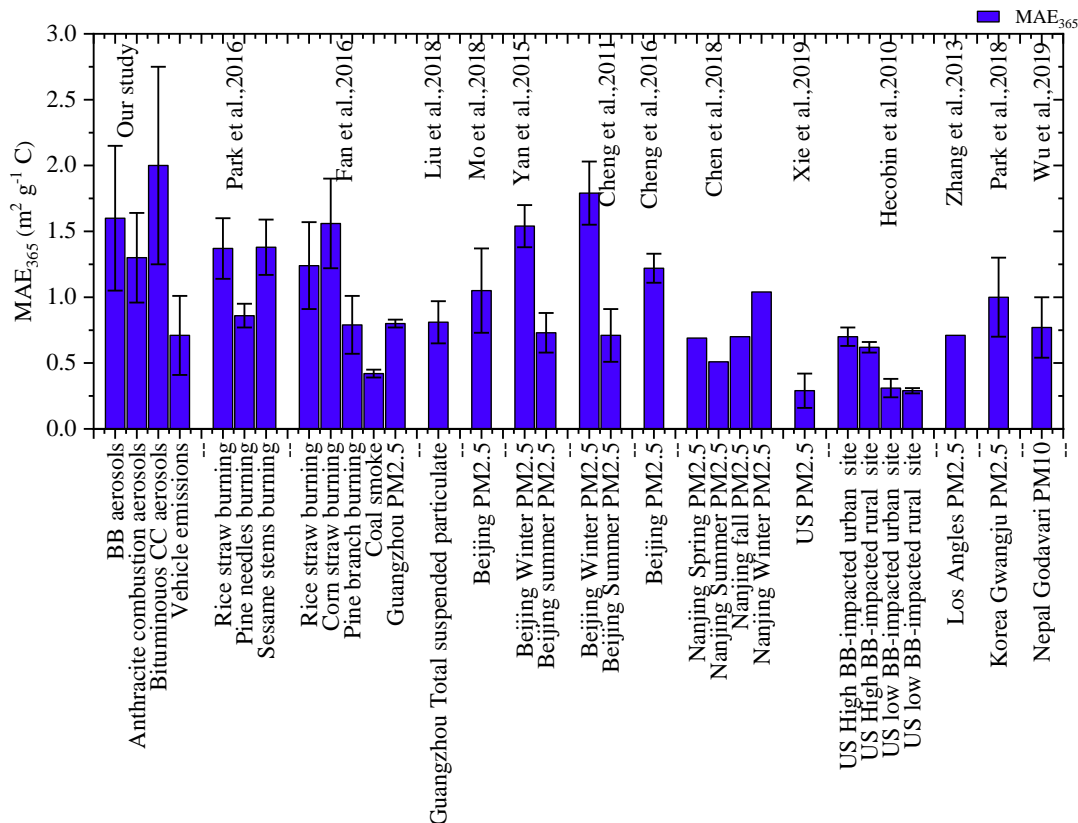


Figure 1. Comparison of MAE₃₆₅ in the WSOC fraction of source emission aerosols with the other studies. The references were as following:(Liu et al., 2018;Mo et al., 2018;Yan et al., 2015;Cheng et al., 2011;Cheng et al., 2016;Xie et al., 2019;Hecobian et al., 2010;Zhang et al., 2013;Park et al., 2018;Wu et al., 2019;Fan et al., 2016;Park and Yu, 2016;Chen et al., 2018).

3.2 EEM spectra of WSOC and MSOC.

Fluorescence spectra was used to characterize the organic chromophores of different sources. We applied the PARAFAC model (Murphy et al., 2013) to determine the underlying chromophore components of the 60 source samples. Six typically independent components in the WSOC were resolved, as shown in the top of Figure 2 and Table 1. Compared with the previous studies, the fluorescence of P1 and P6 were similar to those for 7CM-C1 (the C1 component of a seven-component model) and 7CM-C3, named humic-like substances (HULIS-1) (Chen et al., 2016b). Further, there were peaks in the emission wavelengths (> 400 nm) of P1 and P6, which were probably derived from conjugated systems (Chen et al., 2016b). The peak of P3 component was almost located in the region IV, which was categorized as protein-like

(cytidine) or tryptophan-like fluorophore (Qin et al., 2018;Fan et al., 2016). Generally, peaks at shorter excitation wavelengths (< 250 nm) and shorter emission wavelengths (< 350 nm) were associated with simple aromatic proteins such as tyrosine (Cory and Mcknight, 2005), which was similar to the fluorescence of P2 component observed in this study. P5 component was similar to tryptophan- and tyrosine-like components (Chen et al., 2017a). Therefore, P2, P3, and P5 components were named protein-like substances (PLOM). P4 component was reported relatively rarely but similar to previously observed peaks that were considered to arise mainly in surface water and algal secretions (Yu et al., 2015). It is worth noting that the origins and chemical structures of the chromophores studied are not necessarily like those of chromophores with the same names in other types of organic matter.

Table 1. The maximum excitation and emission wavelengths of the PARAFAC components from the WSOC and MSOC extracted from the three origins

	PARAFAC component	Excitation maxima (nm)	Emission maxima (nm)	Assignment according to published papers	References
WSOC	P1	251, 314	415	HULIS-1, terrestrial humic-like component	(Chen et al., 2016b;Sgroi et al., 2017;Fu et al., 2015)
	P2	254	337	Tyrosine-like	(Cory and Mcknight, 2005)
	P3	287	360	Protein-like (cytidine) or tryptophan-like	(Qin et al., 2018;Fan et al., 2016)
	P4	251	374	-	-
	P5	278	319	Protein-like fluorophores	(Fu et al., 2015)
	P6	254, 371	485	HULIS-1, conjugated systems, a terrestrial humic or fulvic acid-like component	(Chen et al., 2016b)
MSOC	C1	308	356	-	
	C2	<250,272	388		
	C3	<250	434	C2 for the urban ASOM samples	(Matos et al., 2015)

C4	257	360
C5	284	328
C6	269	310

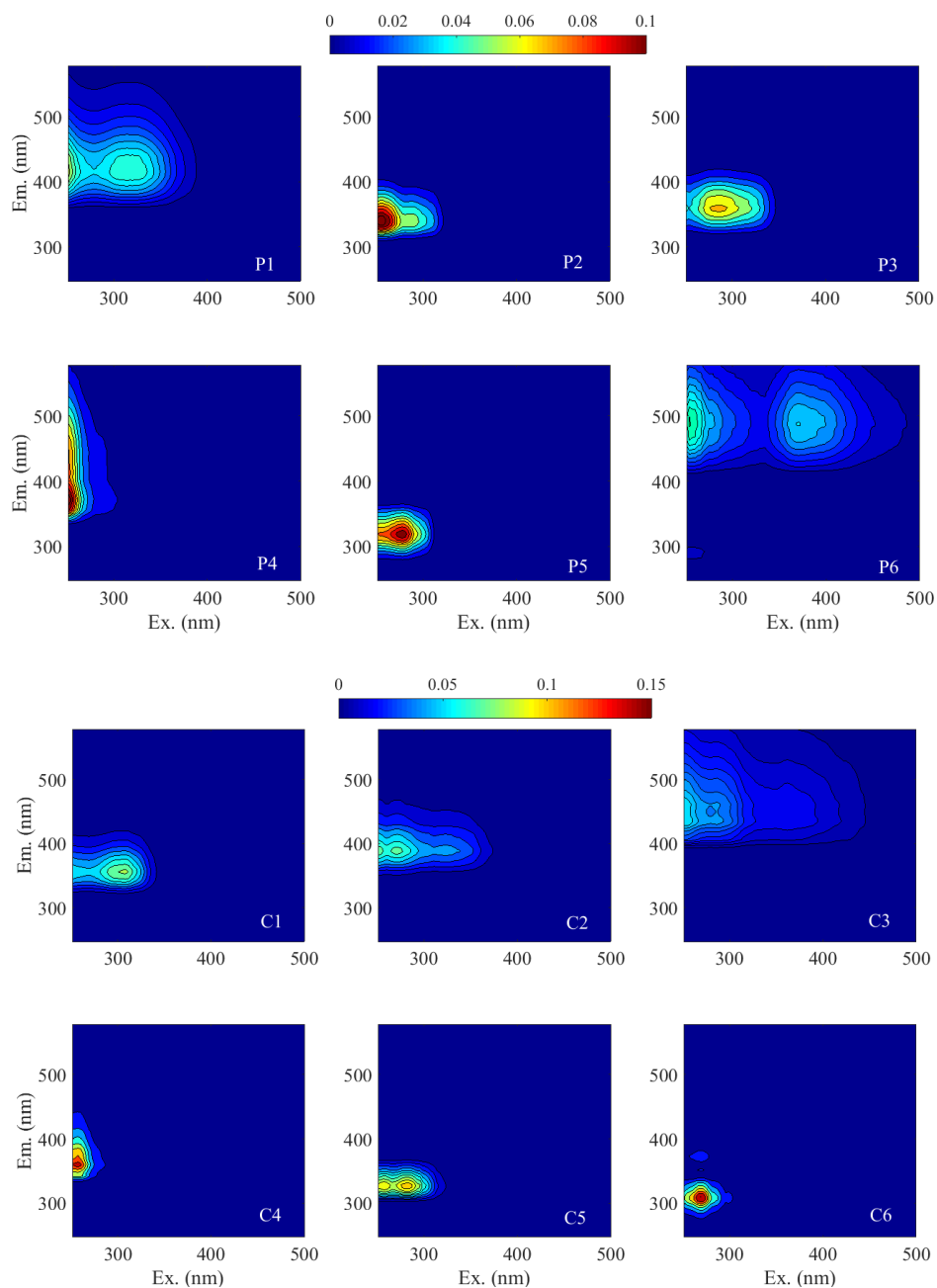


Figure 2. The EEM components identified by PARAFAC of WSOC (top: P1-P6) and MSOC (bottom: C1-C6) extracted from three origins.

The results from the six-component model (abbreviated C1–6) of MSOC identified by PARAFAC, as described in the bottom of Table 1 and Figure 2, were different from those observed in the WSOC, indicating different chemical structures.

The peak of C1 component was similar to that of P3 component of WSOC, but the excitation wavelength was higher than that of P3 component. The higher excitation wavelength indicated the presence of conjugated unsaturated bond systems shifting towards the high wavelengths of C1 component (Matos et al., 2015). Moreover, as reported, C3 component was similar to component 2 of urban alkaline-soluble organic matters (ASOM) collected from the city of Aveiro, Portugal (Matos et al., 2015).

The maximum fluorescence intensity (F_{\max}) was calculated by multiplying the maximum excitation loading and maximum emission loading for each component by its score (Murphy et al., 2013). Generally, changes in the relative abundance of a component ($F_{\max}/\sum F_{\max}$) could indicate changes in its overall importance, which had been successfully applied to study the origins of chromophores (Yan and Kim, 2017; Chen et al., 2017a; Chen et al., 2016b; Wu et al., 2019). In this study, the relative abundances of fluorescent components in different types of samples were highly variable, depending on the sources (Figure 3a). P1 component accounted for an average of $34 \pm 4.7\%$ of the total fluorescence intensities in the case of tunnel aerosols, which was higher than BB aerosols (mean \pm SD: $19 \pm 4.8\%$), CC aerosols ($14 \pm 3.8\%$) and vehicle exhaust particles ($17 \pm 1.0\%$). This result indicated P1 component had an aged vehicle exhaust origin because a difference of P1 component was observed from tunnel aerosols and vehicle exhaust particles. In contrast, the fluorescence of P6 component was weak in any of the samples, but in vehicle emissions ($9.4 \pm 2.3\%$) was higher than BB and CC aerosols (both 2.5%). P5 component was more intense in the vehicle exhaust particles ($30 \pm 1.6\%$) than other sources. P2 component was only abundant in the cases of BB aerosols ($33 \pm 11\%$) but did not exhibit in vehicle emissions, suggested some structures responsible for this chromophore could not exist in vehicle emissions. P4 component was the more abundant chromophore in CC aerosols ($34\% \pm 7.7\%$) and vehicle emissions ($29 \pm 5.9\%$), especially in vehicle exhaust particles ($38 \pm 1.1\%$). In contrast, P4 component in BB aerosols was weak ($11\% \pm 7.9\%$), indicating a fossil origin. P3 component was almost equal across all samples. The possible reason was that P3 component was similar to the peak of tryptophan-like compounds which were common to practically all published models

376 and were likely to be found in almost all sources (Yu et al., 2015).

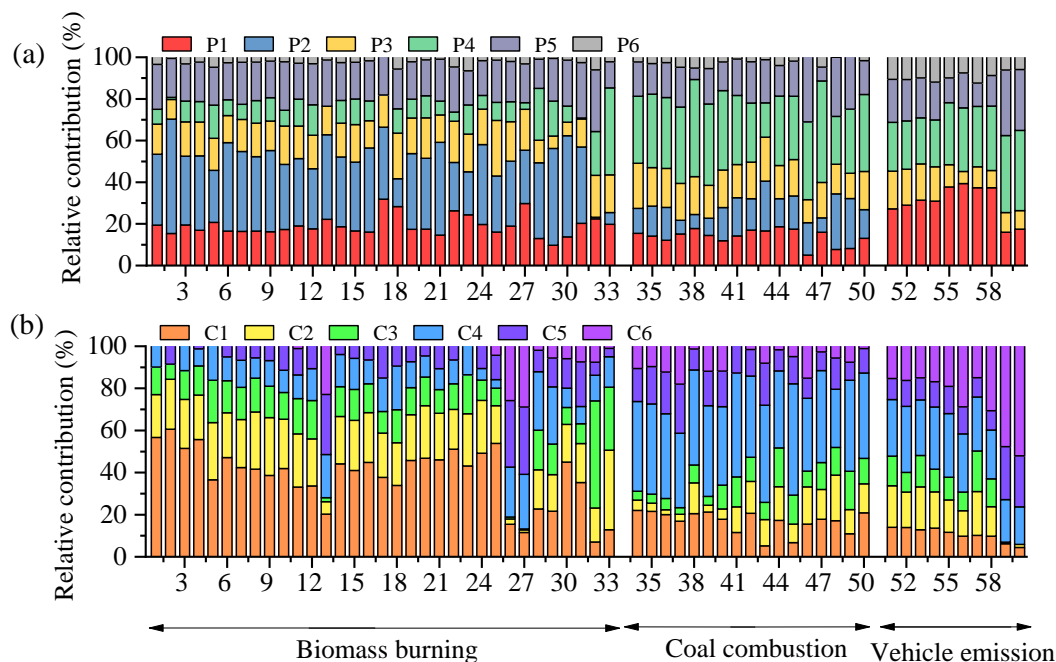


Figure 3. The relative contribution of each PARAFAC component of WSOC (a) and MSOC (b) in the three source emissions.

The relative intensities of fluorescent components in the MSOC exhibited similar characteristics to the WSOC (Figure 3b). C1 component was the substances with more intense in the case of BB aerosols ($38\% \pm 14\%$) than the other sources. C2 component was enriched in BB aerosols ($21\% \pm 6.9\%$) and tunnel aerosols ($17\% \pm 6.9\%$) than those in CC aerosols and vehicle exhaust particles. Also, C2 exhibited a difference between bituminous CC and anthracite combustion aerosols, as well as tunnel aerosols and vehicle exhaust particles, indicating C2 component could be used to identify these sources. C4 component was intense in CC aerosols ($41 \pm 6.0\%$) and vehicle exhaust particles ($25 \pm 4.4\%$). C3 component was not abundant among the three sources and not observed in the vehicle exhaust particles, suggesting not a fresh vehicle-exhaust emission origin. Instead of C3, C5 and C6 components were more intense in vehicle exhaust particles ($25 \pm 6.8\%$ and $50 \pm 6.8\%$, respectively), suggesting they were more primary vehicle emission chromophores. The last study observed that the relative abundances of various chromophores in aerosols with

different particle sizes were different (Chen et al., 2019). Therefore, the fluorescence technique is sensitive for chromophores with different sources, sizes, and chemical structures and so on. Combining these results with the WSOC mentioned above results and comparing the different characteristics and fuel information, the fluorescent components obtained by EEM-PARAFAC could potentially assist with the source apportionment of BrC for environmental applications.

3.3 Molecular composition detected by FT-ICR MS

The molecular composition of WSOC and MSOC extracted from BB and CC aerosols, and vehicle emissions were determined by negative ESI-FT-ICR MS. ESI is a soft ionization method, and it can only ionize polar organic compounds, hydrophilic molecules (Wozniak et al., 2008), but nonpolar or less polar compounds such as polycyclic aromatic hydrocarbons (PAHs) and saturated hydrocarbons are not easily ionized by ESI (Lin et al., 2018). In addition, ESI (-) cannot detect the N-heterocyclic alkaloid compounds (Laskin et al., 2009). Thus, this study mainly discussed these easily ionized polar organic compounds by ESI (-).

Figure 4 showed the reconstructed negative-ion ESI FT-ICR mass spectra of WSOC for the six selected samples. Lots of peaks with an intensive mass range between m/z 150 and 600 were shown in the spectra, with the most massive numbers of ions within the range of m/z 200-400. Additionally, more formulas were detected in BB aerosols (total 7708) than CC aerosols (5305) and vehicle emissions (4047) (Table 2), suggesting a higher observed chemical complexity (i.e., the observed peaks). According to the intensity of each ion, the average molecular formulas of WSOC in the six aerosol samples were calculated and listed as $C_{18.7}H_{23.5}O_{6.99}N_{0.73}S_{0.09}$, $C_{19.9}H_{21.5}O_{7.65}N_{0.34}S_{0.03}$, $C_{16.1}H_{13.3}O_{5.37}N_{0.68}S_{0.23}$, $C_{15.2}H_{13.7}O_{4.24}N_{0.45}S_{0.41}$, $C_{13.4}H_{18.0}O_{7.52}N_{0.45}S_{0.40}$, and $C_{17.3}H_{21.1}O_{5.65}N_{0.53}S_{0.08}$. The BB aerosols had higher contents of C and H, while the CC aerosols and tunnel aerosol had higher contents of S.

Table 2. Number of formulae in each compound category and the average values of elemental ratios, molecular weight (MW), double-bond equivalents (DBE), and aromaticity index (AI_{mod}) in the WSOC from the three origins.

Samples	Elemental composition	Number of formulae	MW_w	DBE_w	$AI_{mod,w}$	O/C_w	H/C_w	DBE/C_w
Musa	Total	4534	372.55	8.36	0.33	0.37	1.25	0.45
	CHO	1504	367.73	8.08	0.32	0.38	1.25	0.43
	CHON	2375	384.06	9.31	0.39	0.34	1.22	0.48
	CHOS	329	320.06	4.59	0.15	0.51	1.46	0.34
	CHONS	323	358.24	5.04	0.12	0.51	1.51	0.35
Hevea	Total	3174	387.05	10.32	0.42	0.38	1.08	0.52
	CHO	1610	377.86	10.06	0.42	0.38	1.08	0.51
	CHON	1408	409.40	11.29	0.46	0.39	1.05	0.55
	CHOS	108	376.68	7.00	0.23	0.38	1.32	0.39
	CHONS	48	410.33	5.08	0.09	0.47	1.60	0.30
Anthracite	Total	3930	308.65	10.82	0.65	0.33	0.83	0.67
	CHO	990	283.07	11.06	0.67	0.28	0.77	0.67
	CHON	1808	323.71	11.67	0.71	0.34	0.81	0.69
	CHOS	464	308.97	8.73	0.49	0.36	0.95	0.59
	CHONS	668	332.83	8.99	0.52	0.46	0.95	0.63
Bituminous coal	Total	1375	282.91	9.63	0.61	0.28	0.90	0.63
	CHO	399	259.21	10.40	0.66	0.22	0.82	0.65
	CHON	411	267.68	9.92	0.69	0.27	0.86	0.67
	CHOS	302	324.65	9.51	0.49	0.28	0.99	0.57
	CHONS	263	299.28	7.98	0.56	0.43	0.98	0.63
Tunnel	Total	2746	317.68	5.68	0.35	0.56	1.34	0.42
	CHO	803	298.29	7.69	0.49	0.50	1.06	0.54
	CHON	1049	340.18	7.50	0.38	0.51	1.22	0.49
	CHOS	508	310.74	2.73	0.03	0.59	1.71	0.23
	CHONS	386	337.90	2.78	0.46	0.81	1.77	0.25
Vehicle exhaust	Total	1301	327.71	7.96	0.41	0.33	1.22	0.46
	CHO	561	311.62	8.02	0.43	0.30	1.19	0.46
	CHON	673	320.62	7.28	0.41	0.40	1.27	0.47
	CHOS	63	467.88	11.88	0.36	0.19	1.19	0.44
	CHONS	4	438.78	2.21	0	0.46	1.97	0.12

In this study, these identified molecular formulas were classified into four main compound groups based on their compositions: CHO, CHON, CHOS, and CHONS. CHO compounds refer to the compounds that contained carbon, hydrogen, oxygen, and the other compound groups that were defined analogously. The relative abundances of the four compound groups were calculated by the magnitude of each peak divided by the sum of magnitudes of all identified peaks and showed in Figure 4. CHO was the most abundant component in the WSOC, accounting for 43% - 69% of total intensities of BB aerosols, 36% - 37% of CC aerosols, and 36% - 47% of vehicle emissions, respectively. CHO in the BB and CC aerosols were lower than those of mass spectra from simulated combustion experiments (BB (53%-72%) and CC (43%)) (Song et al., 2018). Generally, CHO formulas were consistent with species reported previously as lignin-pyrolysis products (Fleming et al., 2017), and they detected this fraction was $43.1\% \pm 14.6\%$ in brushwood-*chulha* cook firers. CHON was abundant in the three sources. This result was different from the findings that CHON species had a higher percentage in BB smoke and were not abundant in CC smoke (Song et al., 2018). The high fraction of CHON in the CC aerosols could be due to that the N-containing compounds in the BB smoke PM_{2.5} come from the nitrogen content in the fuels (Coggon et al., 2016), and the contents in coal fuels were comparable to biomass fuels (See Table S1 and S2). However, S-containing compounds were more abundant in the CC aerosols (9.0%-21% for CHOS and 13%-20% for CHONS, respectively) and tunnel aerosol (24% for CHOS and 16% for CHONS, respectively) than those in the BB aerosols (2.0%-5.6% for CHOS and 0.62%-3.7% for CHONS, respectively) and vehicle exhaust particle (7.5% for CHOS and 0.25% for CHONS, respectively), consistent with the previous studies (Song et al., 2018; Wang et al., 2017). ESI was more efficient in ionizing S-containing compounds and most of them were selectively ionized by ESI-, suggesting that they were polar species such as organosulfates (Lin et al., 2018). Our study reported that S-containing compounds in the WSOC were associated with CC emissions by combining with ¹⁴C data (Mo et al., 2018). Furthermore, the relative abundances of group species in the CC aerosols and TA were similar to those of water extracts in the hazy day (Jiang et al., 2016), indicating both sources could be the important contributors of haze. However, differences between tunnel aerosol and vehicle exhaust particle were observed, indicating S-containing compounds in the tunnel aerosol were more secondary formation.

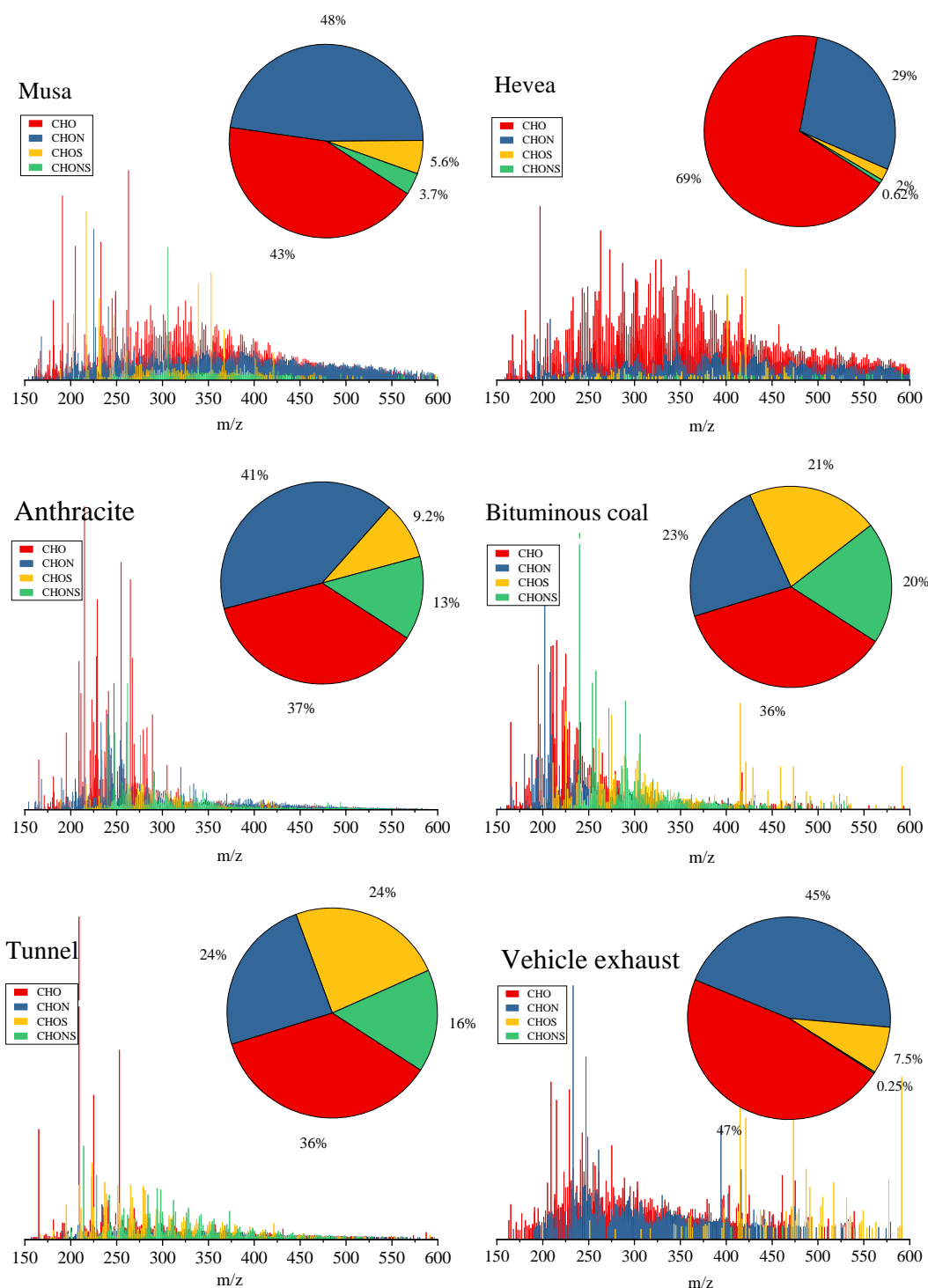


Figure 4. Negative ESI FT-ICR mass spectra of WSOC in the six aerosol samples. Different formula groups were color-coded. The six pie charts showed the relative intensities of different formula groups.

Van Krevelen (VK) diagram is a useful tool that provides a visual graphic display of compound distribution, and to some extent, use to qualitatively identify different composition domains in organic mixtures (Song et al., 2018;Lv et al., 2016;Smith et al., 2009). In this study, each source showed similar VK patterns. Musa

and Hevea burning had a resemble VK diagram to that of WSOC in straw burning and fog water (Schmitt-Kopplin et al., 2010; Mazzoleni et al., 2010). S-containing compounds in tunnel aerosol with high O/C and H/C ratio were similar to the aerosol-derived WSOC in New York and Virginia (Wozniak et al., 2008). Six dominate domains were identified in the WSOC, including lignins, carbohydrates, tannins, proteins, condensed aromatic, and unsaturated hydrocarbons. As shown in Figure S9, results showed compounds observed in the CC aerosols had lower H/C and O/C ratios than those in the BB aerosols and vehicle emissions, indicating a higher unsaturated degree and lower oxidation level. There were compounds outside the specified regions, which had a high H/C ratio (≥ 2.2), and DBE = 0 correspond to saturated oxygenated species and could be some long-chain polyalcohols (Lin et al., 2012a).

The mass spectra of MSOC exhibited differences from WSOC (Figure S10), especially in the BB aerosols and vehicle emissions that exhibited larger m/z in the range of 350-600. The detected formulas in the MSOC were much lower than those in the WSOC, with the number of 4502, 3628, and 1069 for the BB, CC, and vehicle emission aerosols, respectively. The reason could be due to that ESI can efficiently ionize the polar compounds, and the methional extracts after water-extracted may contain more moderate- and low- polar compounds that were not easily ionized. The average molecular formulas were $C_{26.9}H_{46.2}O_{4.27}N_{0.24}S_{0.02}$, $C_{23.3}H_{34.9}O_{5.18}N_{0.20}S_{0.02}$, $C_{18.2}H_{19.2}O_{4.24}N_{0.92}S_{0.03}$, $C_{22.4}H_{20.7}O_{3.01}N_{0.38}S_{0.05}$, $C_{22.6}H_{44.1}O_{5.70}N_{0.74}S_{0.11}$, and $C_{25.2}H_{48.5}O_{4.86}N_{0.58}S_{0.08}$ of MSOC in the six aerosol samples, respectively, showing higher C and H contents than their corresponding formulas of WSOC but a decreasing trend in the O contents.

CHO and CHON were the main components in the MSOC, accounting for about 90% of the total intensities (CHO plus CHON). CHO was the most abundant category observed in the BB aerosols (78%-80%). The elemental compositions observed in CC aerosols were different between bituminous coal and anthracite combustion, where the latter had more abundance of CHON (73%), but the former with more CHO (60%), which was consistent with their corresponding WSOC and could be due to anthracite had higher N content but lower O content than bituminous coal (see Table S2). However, CHON in the BB aerosols (18%-20%) exhibited lower abundance than those in the CC aerosols and vehicle emissions. These results provided a new sight for those CHON compounds that contributed to a high abundance in fossil fuel

combustion in the MSOC. Besides, S-containing compounds were not abundant in the MSOC. It is potential to due to that S element combined with O atom may exhibit higher polarity.

Figure S11 showed the VK diagram of MSOC in the six aerosol samples. More formulas in BB aerosols exhibited two distinct groups with H/C 1.4-2.2 and 0.6-1.4 vs. O/C 0.1-0.5, inside three domains (lignins, proteins, and lipids). Compounds in CC aerosols with lower H/C and O/C ratios were dominant in the domains of lignins and condensed aromatic, especially in the bituminous CC aerosol with more unsaturated hydrocarbon. Tunnel aerosol showed a wide range of O/C in S-containing compounds and a wide range of H/C in non-S-containing compounds. In contrast, compounds in vehicle exhaust particle had a wide range of H/C but a narrow O/C ratio. The VK diagram with fewer S-containing compounds in the vehicle exhaust particle showed a similar characteristic to the distribution of non-S-containing compounds in tunnel aerosol, indicating the difference was mainly due to the S-containing compounds.

Table 2 and S5 presented the relative abundance weighted molecular weight (MW_w), Double bonds equivalence (DBE_w), and modified aromaticity index ($AI_{mod,w}$) of WSOC and MSOC, respectively (see SI). DBE was used as a measure of unsaturated level in a molecule, and AI_{mod} could be used to estimate the fraction of aromatic and condensed aromatic structures (Song et al., 2018;Lv et al., 2016;Koch and Dittmar, 2006). BB aerosols had higher MW_w values than CC and vehicle emissions in the WSOC. Besides, higher DBE_w and $AI_{mod,w}$ values were observed in the CC aerosols than the other two sources. MSOC had higher MW_w but lower AI_{mod} values (except for CC aerosols) than the corresponding WSOC. Furthermore, CHO and CHON compounds had higher DBE_w and $AI_{mod,w}$ values than S-containing substances, consistent with the earlier results (Lin et al., 2012b;Lin et al., 2012a).

Figure S12 showed the fraction of AI_{mod} values of WSOC in the six aerosol samples, where the formulas were classified according to their AI_{mod} (aliphatic ($AI = 0$), olefinic ($0 < AI \leq 0.5$) and aromatic ($AI > 0.5$)). The results illustrated that the fraction of aromatic structure in non-S-containing compounds was higher than those in S-containing compounds. CC aerosols had a higher aromatic fraction than BB aerosols and vehicle emissions, especially in CHO and CHON (up to 89% of total ion intensities). In the BB aerosols, the non-S-containing compounds had a high fraction of olefinic structure, following by aromatic structure, but the S-containing compounds had a higher aliphatic and olefinic structure than aromatic structure. Besides, a higher

fraction of aliphatic in vehicle emissions was observed in S-containing compounds (especially in tunnel aerosol (exceed 81%)). These aliphatic S-containing compounds might form by the precursors (long-chain alkanes) from vehicle emissions (Tao et al., 2014), which had higher H/C and lower DBE values (see Table 2). However, the previous study showed that AI must be regarded as the most conservation approach and may result in an underestimate of the aromatic structures (Koch and Dittmar, 2006), which was observed in Beijing aerosols (Mo et al., 2018). Although AI_{mod} identified more compounds as aromatic and condensed aromatic components than AI, the AI_{mod} may introduce uncertainties for individual molecules, which was demonstrated by Koch and co-author.

Consistent with WSOC, high fractions of the aromatic structure were observed in non-S-containing compounds than S-containing compounds, and higher fractions of aromatic structure in the CC aerosols were observed than BB aerosols and vehicle emissions in the MSOC (Figure S13). Furthermore, we found that the fraction of aliphatic in MSOC was higher than that in WSOC, indicating more fat-like compounds.

Different chemical characteristic of BB, CC, and vehicle emissions

Figure S14 plotted the Venn diagram of formulas in the WSOC fraction in the six aerosol samples for determining the unique elementals in the mass spectra. The previous study identified the unique elementals of water-soluble HULIS in simulated BB and CC smokes, which presented different molecular characteristics between biomasses, as well as between biomass and coal (Song et al., 2018). In this study, we combined more formulas of different sources to determine the unique molecular and more limitation was set, which would provide more identified characteristics for each source. 212 molecular formulas were detected simultaneously in the six aerosol samples, suggesting the compounds could be more detected in the atmosphere. It is noting that without any further information, it is not possible to decide whether these common formulas represent the same compounds. There were 112 of CHO unique molecular in 212 and 98 of CHON but only 2 of CHOS molecular. CHO compounds were relatively small aromatic compounds with 8-10 C atoms and 3-8 O atoms and DBE 5-13 and multiple acidic polar functional groups (Figure S15). It is noting that lines in Figure S15 indicate DBE reference values of linear conjugated polyenes C_xH_{x+2} with $DBE=0.5 \times C$, and fullerene-like hydrocarbons with $DBE=0.9 \times C$, where

the data points inside this region are potential BrC chromophores (Lin et al., 2018). For example, organic acids ($C_8H_6O_5$ (DBE=6)) was detected in Urban $PM_{2.5}$ (Yassine et al., 2012), as well as $C_9H_8O_5$ (6), $C_{14}H_{14}O_4$ (8), $C_{13}H_{14}O_5$ (7), which allowed them to ionization in the ESI- mode and were identified as potential BrC chromophores. In total, all of CHON compounds had $O/N \geq 2$ (5.3 ± 1.28 , 2.5-7) (Figure S15), allowing for the assignment of at least one nitro ($-NO_2$) or nitrooxy ($-ONO_2$) group and other oxygen-containing groups (i.e., $-OH$ and $-COOH$). Except for $C_{19}H_{41}O_7N$ (DBE=0), the remaining compounds with $DBE \geq 5$ were suggested as nitro-aromatic and nitrophenol derivatives (Mo et al., 2018; Lin et al., 2018). CHOS species only had two formulae including $C_{18}H_{38}O_7S$ (0) and $C_{20}H_{38}O_7S$ (2). It was reported that O_7S groups were the most abundant species class in CHOS identified in water extracts of $PM_{2.5}$ (Jiang et al., 2016).

There were more observed unique peaks of WSOC in the BB aerosols (total 1947) compared to CC aerosols (1583) and vehicle emissions (813). However, only 143 and 83 molecular were identified in bituminous CC and vehicle exhaust particle, respectively. Among the observed compounds, 1353 and 1440 unique molecular formulas were detected in combustion of Musa and anthracite, respectively, showing a significant difference from the others. Figure 5 (a) showed the VK diagram of these unique formulas of WSOC for each sample, where four regions were circled for representing different sources. The results indicated that these unique compounds in different sources had a distinctive chemical characteristic. That may be the reason that resulted in variable fluorescent spectra in different sources (discussed above). Additionally, the diagram showed that the unique molecular in CC aerosols located in the region with lower H/C and O/C, and vehicle emissions between tunnel aerosol and vehicle exhaust particle located in two distinct regions.

Figure 6 showed plots of the DBE vs. the number of carbon atoms in the unique molecular formulas of all aerosol samples. These compounds observed in the BB aerosols were largely CHO and CHON (CHO and CHON, 88% - 93%) with C numbers ranging from 6 to 40 and DBE ranging from 0 to 31, with no regular distribution. S-containing compounds were the important components in the unique molecular formulas of CC aerosols (CHOS and CHONS, 38%-75%) and vehicle emissions (CHOS and CHONS, 41%-66%). However, only 7%-12% of the total unique molecular formulas were observed in BB aerosols. As shown in Figure 6, the

region marked by blue box denoted the high intensities of compounds in unique formulas of each sample. The high-intensity compounds detected in the Musa burning aerosol were mainly C number from 14 to 24, DBE from 7 to 13, and two N atoms, such as $C_{20}H_{26}O_7N_2$ (9), $C_{18}H_{24}O_2N_2$ (8), $C_{22}H_{28}O_6N_2$ (10), $C_{19}H_{26}O_7N_2$ (8), $C_{21}H_{28}O_6N_2$ (7), $C_{14}H_{18}O_7N_2$ (7), $C_{24}H_{30}O_8N_2$ (11), and $C_{21}H_{24}O_5N_2$ (11) and so on. Instead of Musa, the abundant compounds in the Hevea were mainly $C_{24}H_{22}O_9$ (14), $C_{28}H_{28}O_{11}$ (15), and $C_{28}H_{26}O_{11}$ (16), and so on. Although the difference between burning of Musa and Hevea appeared, the VK diagram (Figure 5) did not show distinct changes. The high-intensity compounds in the anthracite combustion with lower C atoms than in the bituminous CC, which were main $C_{14}H_8O_5N_2$ (12), $C_{12}H_{11}O_4NS$ (8), $C_{12}H_{10}O_8N_2$ (9), while in bituminous CC were main $C_{28}H_{28}O_4S$ (15) and its homolog of $C_{27}H_{26}O_4S$ (15), and $C_{19}H_{16}O_3S$ (12). The abundant compounds in tunnel aerosol had a lower unsaturation degree, such as $C_4H_9O_7NS$ (1), $C_5H_{11}O_7NS$ (1), $C_7H_{13}O_5S$ (1). In the vehicle exhaust particle, the high intensity of compounds was one fraction with low C atoms and DBE ($C_{21}H_{40}O_8N_2S$ (3), $C_{26}H_{46}O_3S$ (4)), and the other fraction with high C atoms and DBE ($C_{32}H_{34}O_8S$ (16), $C_{30}H_{34}O_5S$ (14)). These findings are essential because these unique molecular formulas in different sources may have specific chemical composition, which would help the source apportionment of aerosols.

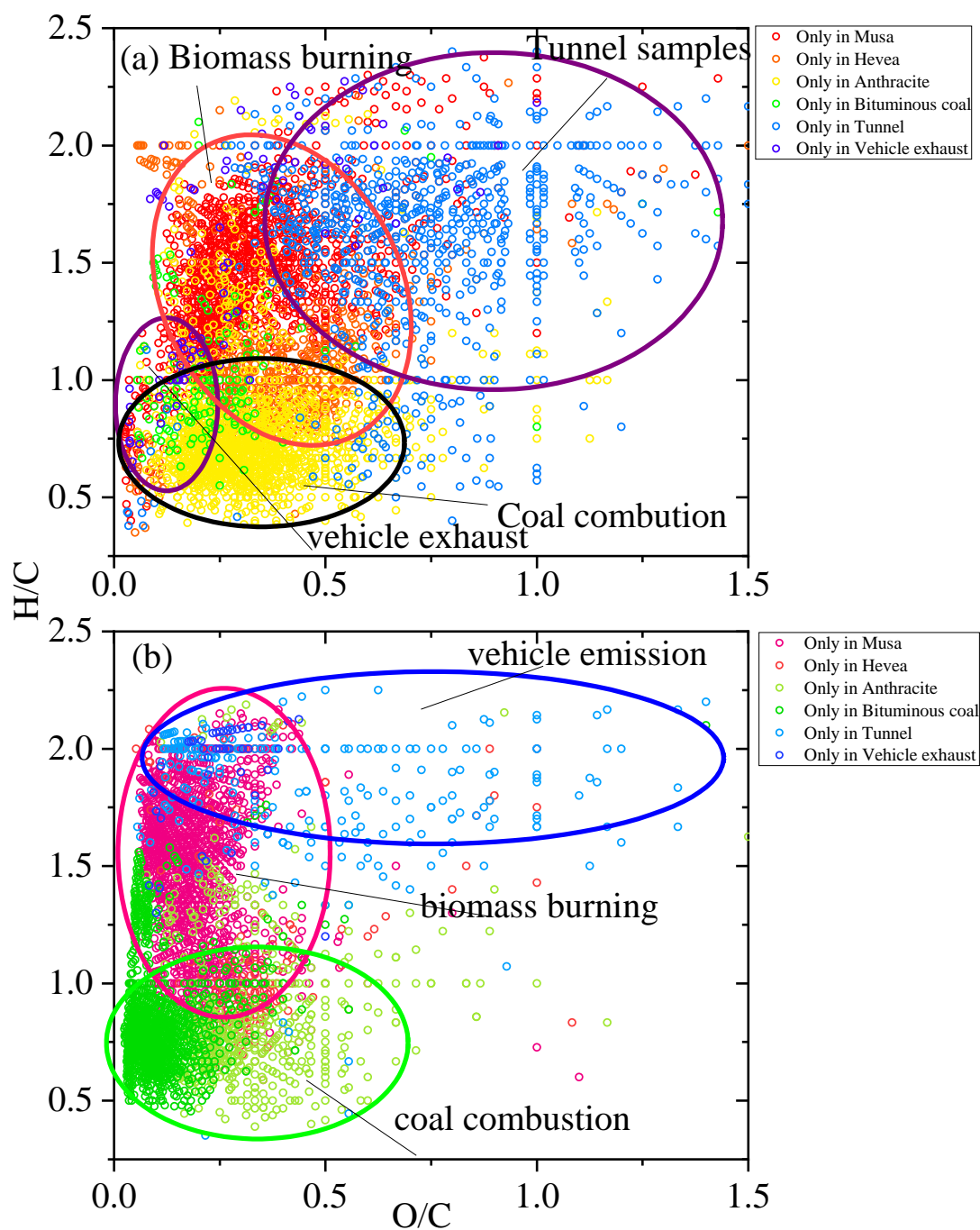


Figure 5. A Van Krevelen diagram of WSOC (a) and MSOC (b) in the six samples. Different color indicates unique formulas detected in each sample.

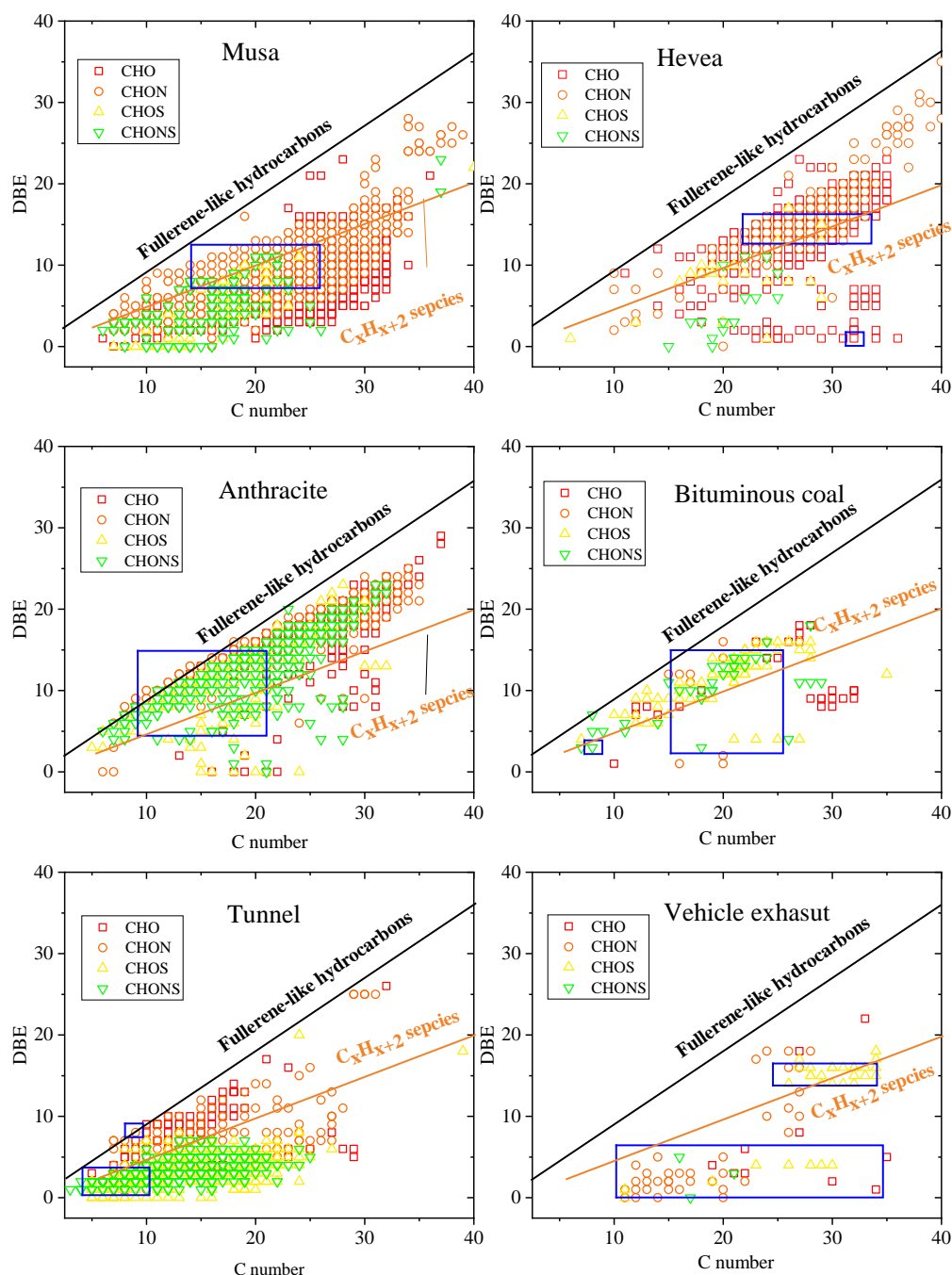


Figure 6. DBE vs. C number for unique molecular compounds of WSOC for the six aerosol samples. Lines indicate DBE reference values of linear conjugated polyenes C_xH_{x+2} with $DBE=0.5 \times C$, and fullerene-like hydrocarbons with $DBE=0.9 \times C$. The regions marked by blue box denoted the high intensities of compounds.

Comparison with WSOC, Figure S16 showed fewer compounds in common in the MSOC for the six aerosol samples. There were only 44 compounds common in the six aerosol samples. A total of 26 and 14 of the 44 formulas were CHO and CHON, respectively, but only 4 of the 44 formulas were S-containing compounds. As shown

in Figure S17, there were only three compounds ($C_{17}H_8O_2$ (13), $C_{18}H_{14}O$ (12), $C_{18}H_{12}O_2$ (13)) in CHO group, and one compound ($C_{14}H_{11}O_4N$ (10)) in CHON group inside the potential BrC region. The remaining compounds had a high C number (18-35), low O atoms (1-7), and low DBE (0-2), suggesting that they mostly had fatty acid structures.

These unique molecular in VK also showed similar results comparing to WSOC (Figure 5 (b)), further confirming the special characters in different sources. Expect for tunnel aerosol (about 50%), these unique formulas in the BB aerosols, CC aerosols, and vehicle exhaust particle was dominant by CHO- and CHON-groups (Figure S18), indicating S-containing compounds with lower polarity could be originated from the secondary formation of vehicle exhaust. The high-intensity compounds were $C_{35}H_{69}O_5N$ (2), $C_{38}H_{76}O_4$ (1) for Musa burning; $C_{26}H_{22}O_7$ (16), $C_{28}H_{26}O_7$ (16) for Hevea burning; $C_{14}H_{12}O_6N_2$ (10), $C_{17}H_{14}O_5N_2$ (12) for anthracite combustion; $C_{23}H_{16}O$ (16), $C_{24}H_{18}O$ (16), $C_{24}H_{14}O$ (18) for bituminous CC; $C_4H_9O_7NS$ (1), $C_{24}H_{42}O_3S$ (4), $C_8H_{16}O_5S$ (1) for tunnel aerosol, and $C_{26}H_{37}O_5NS$ (7), $C_{22}H_{46}O_7$ (0) for vehicle exhaust particle, respectively.

3.4 Link of molecular composition and optical properties

In the above statements, we discussed the light absorption and fluorescence properties from aerosols in the three different sources. The light absorption capacity of WSOC and MSOC was essential to assess the evolution of BrC, and fluorescence spectra were sensitive to different sources and could help for the source apportionment of BrC. Besides, we evaluated the molecular composition of the three sources. Therefore, understanding the factors affecting the optical properties of BrC is important. It was reported that the MAE in the BB experiments depended largely on burning conditions (Chen and Bond, 2010) and in the CC experiments depended on coal maturity (Li et al., 2018). Chen et al., (2017b) illustrated that higher light absorption capacity were associated with low- and medium-polar fractions that contained aromatic and polar functional groups (O or both O and N atoms). Sources play an important role in light absorption capacity, consistent with our current study. The MAE₃₆₅ values of WSOC in highly BB-impacted areas were two times higher than in low BB-impacted areas in the Southeastern United States (Hecobian et al., 2010). Atmospheric aging has a significant effect on the light absorption capacity of BrC (Li et al., 2019), but the mechanism involved is very complex. The response of

the light absorption capacity of different types of BrC to aging is highly variable, and enhancement or reduction in the light absorption capacity of BrC is possible (Li et al., 2019). These results indicated that light absorption capacity might be affected by various factors. In this study, higher MAE₃₆₅ values were observed in the BB and CC aerosols than vehicle emissions, and the chemical structures and unsaturation degree of different sources were discussed. Next, we further discussed the relationships between optical properties and chemical structures.

In order to reduce the influence of non-absorbing substances, we firstly determined these compounds, which were potential to absorb light radiation based on the above statement. Mo et al., (2018) reported that MAE₃₆₅ of HULIS in aerosols was affected by oxidation level and unsaturation degree. In this study, the MAE₃₆₅ had no significant correlation with O/C, indicating that light absorption capacity does not appear to be affected by their oxidized properties in the source aerosols. Instead of O/C, the MAE₃₆₅ had a well positive correlation with the average DBE and MW, respectively (Figure 7), suggesting the unsaturation level and MW played a vital role in the light absorption capacity of source samples. Field experiments indicated that the majority of absorption was the larger molecules (>500 Da) (Di Lorenzo et al., 2017). It is crucial to knowledge the relationship between light absorption of source samples and their molecular composition due to the compounds in fresh emissions that may undergo a secondary process and introduce more uncertainty for their optical properties.

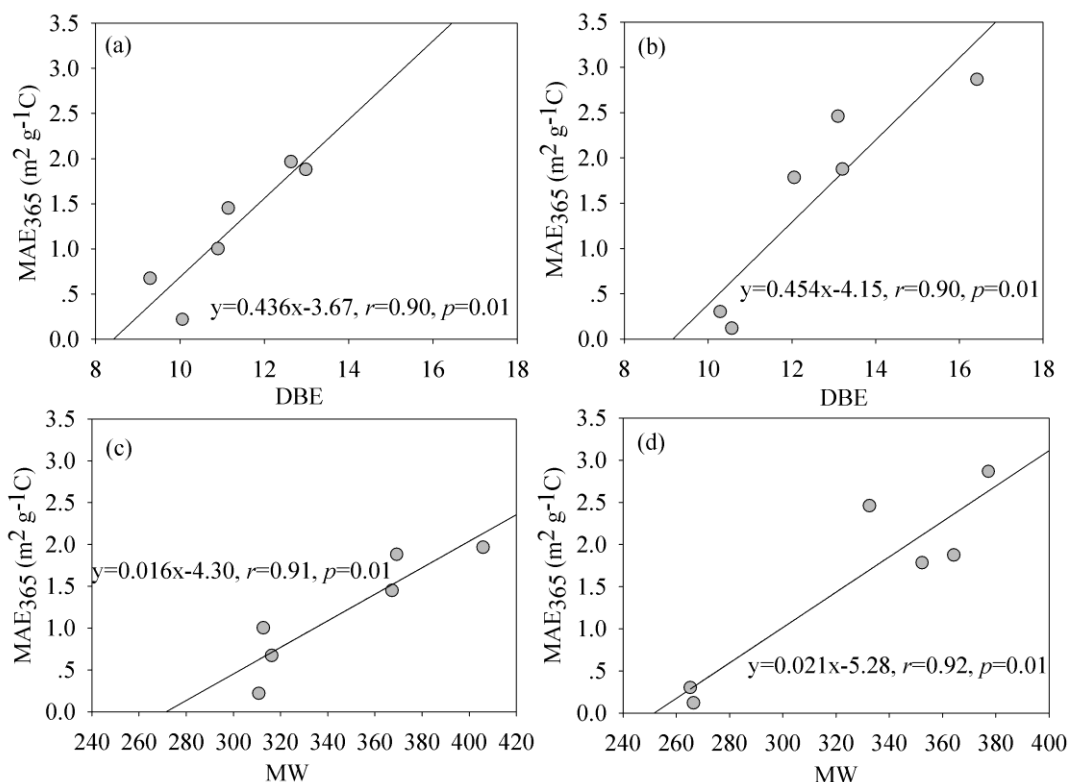


Figure 7. Relationship between DBE and MW of the potential BrC molecules and the MAE₃₆₅ of WSOC (a, c) and MSOC (b, d) in the six samples, respectively.

Fluorescence spectra could provide more information than UV-vis spectra. A red shift in the excitation/emission maximum could indicate increased aromaticity and higher molecular weight (Ghidotti et al., 2017). Field observation had demonstrated that chromophore components were associated with chemical structures (Chen et al., 2016b; Chen et al., 2016a; Stubbins et al., 2014). Chen et al., (2016b) illustrated that the fluorescent components of HULIS-1 and HULIS-2 were correlated positively with CO⁺ and CO₂⁺, and C_xH_y⁺ and C_xH_yO₁⁺ groups ions, respectively, using the correlation analysis of the relative intensities of ion groups in the high-resolution aerosol mass spectrometers (HR-AMSs) and relative contents of fluorescence components. In another study, Chen et al., (2016a) demonstrated that fluorescent components had strong links with chemical groups in the Fourier transform infrared (FT-IR) spectra, including the oxygenated functional groups (nonacidic carbonyl C=O and carboxylic COOH groups), aliphatic C-H group, amine C-NH₂, and alcohol C-OH groups. The chromophores are sensitive to sources, and it is very important to understand the molecular composition of chromophores for classification and source apportionment of atmospheric BrC. However, the ESI- cannot ionize the most typical BrC chromophores such as O-heterocyclic PAHs (O-PAHs), N-heterocyclic PAHs

(O-PAHs) (Lin et al., 2018), which was not enough to discuss the relationship between the fluorescence spectra and molecular composition. The combination of atmospheric pressure photoionization (APPI+ and APPI-) and ESI (+ and -) may provide more ionized compounds, but these techniques were not within the scope of our study.

4 Conclusions

We conducted comprehensive measurements on light absorption, fluorescence, and molecular compositions of dissolved BrC derived from smoke particles during the simulated combustion of biomass and coal, as well as vehicle emission aerosols. We observed BB and CC aerosols had high MAE_{365} values than vehicle emissions, on average, 1.6 ± 0.55 , 1.3 ± 0.34 , 2.0 ± 0.75 , and $0.71 \pm 0.30 \text{ m}^2 \text{ g}^{-1} \text{ C}$ for BB, anthracite combustion, bituminous CC and vehicle emission aerosols, respectively. In addition, BrC emitted from BB ($2.3 \pm 1.1 \text{ m}^2 \text{ g}^{-1} \text{ C}$) and bituminous CC ($3.2 \pm 1.1 \text{ m}^2 \text{ g}^{-1} \text{ C}$) in the MSOC exhibited stronger light absorption capacity than those in the WSOC, but opposite results were found in anthracite combustion aerosols ($0.88 \pm 0.74 \text{ m}^2 \text{ g}^{-1} \text{ C}$) and vehicle emissions ($0.26 \pm 0.09 \text{ m}^2 \text{ g}^{-1} \text{ C}$). EEM combining with PARAFAC analysis determined six types of fluorescent components that were assigned as two HULIS-1 (P1, and P6), three PLOM (P2, P3, P5), and one undefined (P4) in the WSOC in the source samples. The relative intensities of the fluorescent components mainly depended on the different types of sources. For example, HULIS-1 was abundant in tunnel aerosols, P2 was more intense in BB aerosols but not observed in vehicle emissions, P4 was intense in CC aerosols and vehicle emissions, P5 was more abundant in the fresh vehicle exhaust particles; although P3 was not abundant it was ubiquitous in all tested aerosols. Similar to WSOC, six fluorescent components were identified in MSOC. Although the methanol-soluble chromophores were poorly understood, different characteristics were observed in different sources.

FT-ICR mass spectra showed that the m/z of the mainly compounds with m/z 200-400 in the WSOC and MSOC was m/z 350-600 (except for CC aerosols), respectively. CHO and CHON were the main components in the three origins, but S-containing compounds were more abundant in CC and tunnel aerosols than BB aerosols and vehicle exhaust particles in the WSOC. Similarly, MSOC mainly also contained CHO and CHON species but fewer S-containing compounds. BB aerosols had higher CHO species in MSOC but showed lower CHON than CC aerosols and

vehicle emissions. Ven diagram showed that CC aerosols had more unsaturation degree and low oxidation level than the other two sources. This finding was further confirmed by a higher fraction of aromatic in CC aerosols. Unique formulas determined by Venn diagram showed certain specific chemical characteristics in VK diagram. BB aerosols emitted unique formulas with more CHO and CHON (88%-93%), while CC aerosols and vehicle emissions contained more S-containing compounds (38%-75% and 41%-46%, respectively). The relationship between optical properties and chemical structures showed the light absorption capacity was positively associated with an unsaturation degree and MW in the source emissions. Our study illustrated the important roles of sources in light-absorbing BrC and molecular compositions, and the EEMs-based and molecular-characteristic-based method for classification and source apportionment of chromophores in atmospheric aerosols.

Data availability. The data used in this study are available upon request; please contact Gan Zhang (Zhanggan@gig.ac.cn) and Jun Li (junli@gig.ac.cn)

Supplement. The supplement related to this article is available.

Author contributions. JT, GZ, JL, and YC designed the experiment. JT and MC carried out the measurements and analyzed the data. JT, TS, YH, and HJ organized and performed the samplings. JT (Jianhui Tang) and BJ supported the fluorescence and FT-ICR MS instrument. JT wrote the paper. JL, YM, JS, PP, and GZ reviewed and commented on the paper.

Competing interests. The authors declare that they have no conflict of interest.

Acknowledgements. This study was supported by the Natural Science Foundation of China (NSFC; Nos. 41430645 and 41773120), the National Key R&D Program of China (2017YFC0212000), and the International Partnership Program of Chinese Academy of Sciences (Grant No.132744KYSB20170002).

Reference:

- Andersson, C. A., and Bro, R.: The N-way Toolbox for MATLAB, Chemom. Intell. Lab. Syst., 52, 1-4, [https://doi.org/10.1016/s0169-7439\(00\)00071-x](https://doi.org/10.1016/s0169-7439(00)00071-x), 2000.
- Andrade-Eiroa, Á., Canle, M., and Cerdá, V.: Environmental Applications of Excitation-Emission

- Spectrofluorimetry: An In-Depth Review I, *Appl. Spectrosc. Rev.*, 48, 1-49, <https://doi.org/10.1080/05704928.2012.692104>, 2013.
- Bahram, M., Bro, R., Stedmon, C., and Afkhami, A.: Handling of Rayleigh and Raman scatter for PARAFAC modeling of fluorescence data using interpolation, *J. Chemom.*, 20, 99-105, <https://doi.org/10.1002/cem.978>, 2006.
- Bhattacharya, R., and Osburn, C. L.: Multivariate Analyses of Phytoplankton Pigment Fluorescence from a Freshwater River Network, *Environ. Sci. Technol.*, 51, 6683-6690, <https://doi.org/10.1021/acs.est.6b05880>, 2017.
- Budisulistiorini, S. H., Riva, M., Williams, M., Chen, J., Itoh, M., Surratt, J. D., and Kuwata, M.: Light-Absorbing Brown Carbon Aerosol Constituents from Combustion of Indonesian Peat and Biomass, *Environ. Sci. Technol.*, 51, 4415-4423, <https://doi.org/10.1021/acs.est.7b00397>, 2017.
- Chen, H., Liao, Z. L., Gu, X. Y., Xie, J. Q., Li, H. Z., and Zhang, J.: Anthropogenic Influences of Paved Runoff and Sanitary Sewage on the Dissolved Organic Matter Quality of Wet Weather Overflows: An Excitation-Emission Matrix Parallel Factor Analysis Assessment, *Environ. Sci. Technol.*, 51, 1157-1167, <https://doi.org/10.1021/acs.est.6b03727>, 2017a.
- Chen, Q., Ikemori, F., and Mochida, M.: Light Absorption and Excitation-Emission Fluorescence of Urban Organic Aerosol Components and Their Relationship to Chemical Structure, *Environ. Sci. Technol.*, 50, 10859-10868, <https://doi.org/10.1021/acs.est.6b02541>, 2016a.
- Chen, Q., Miyazaki, Y., Kawamura, K., Matsumoto, K., Coburn, S., Volkamer, R., Iwamoto, Y., Kagami, S., Deng, Y., Ogawa, S., Ramasamy, S., Kato, S., Ida, A., Kajii, Y., and Mochida, M.: Characterization of Chromophoric Water-Soluble Organic Matter in Urban, Forest, and Marine Aerosols by HR-ToF-AMS Analysis and Excitation-Emission Matrix Spectroscopy, *Environ. Sci. Technol.*, 50, 10351-10360, <https://doi.org/10.1021/acs.est.6b01643>, 2016b.
- Chen, Q., Ikemori, F., Nakamura, Y., Vodicka, P., Kawamura, K., and Mochida, M.: Structural and Light-Absorption Characteristics of Complex Water-Insoluble Organic Mixtures in Urban Submicrometer Aerosols, *Environ. Sci. Technol.*, 51, 8293-8303, <https://doi.org/10.1021/acs.est.7b01630>, 2017b.
- Chen, Q., Mu, Z., Song, W., Wang, Y., Yang, Z., Zhang, L., and Zhang, Y. L.: Size - Resolved Characterization of the Chromophores in Atmospheric Particulate Matter From a Typical Coal - Burning City in China, *Journal of Geophysical Research: Atmospheres*, 124, 10546-10563, <https://doi.org/10.1029/2019jd031149>, 2019.
- Chen, Y., Sheng, G., Bi, X., Feng, Y., Bixian Mai, A., and Fu, J.: Emission Factors for Carbonaceous Particles and Polycyclic Aromatic Hydrocarbons from Residential Coal Combustion in China, *Environ. Sci. Technol.*, 39, 1861, <https://doi.org/10.1021/es0493650>, 2005.
- Chen, Y., and Bond, T. C.: Light absorption by organic carbon from wood combustion, *Atmos. Chem. Phys.*, 10, 1773-1787, [10.5194/acp-10-1773-2010](https://doi.org/10.5194/acp-10-1773-2010), 2010.

- Chen, Y., Tian, C., Feng, Y., Zhi, G., Li, J., and Zhang, G.: Measurements of emission factors of PM_{2.5}, OC, EC, and BC for household stoves of coal combustion in China, *Atmos. Environ.*, 109, 190-196, <https://doi.org/10.1016/j.atmosenv.2015.03.023>, 2015.
- Chen, Y., Ge, X., Chen, H., Xie, X., Chen, Y., Wang, J., Ye, Z., Bao, M., Zhang, Y., and Chen, M.: Seasonal light absorption properties of water-soluble brown carbon in atmospheric fine particles in Nanjing, China, *Atmos. Environ.*, 230-240, <https://doi.org/10.1016/j.atmosenv.2018.06.002>, 2018.
- Cheng, Y., He, K. B., Zheng, M., Duan, F. K., Du, Z. Y., Ma, Y. L., Tan, J. H., Yang, F. M., Liu, J. M., Zhang, X. L., Weber, R. J., Bergin, M. H., and Russell, A. G.: Mass absorption efficiency of elemental carbon and water-soluble organic carbon in Beijing, China, *Atmos. Chem. Phys.*, 11, 11497-11510, [10.5194/acp-11-11497-2011](https://doi.org/10.5194/acp-11-11497-2011), 2011.
- Cheng, Y., He, K.-b., Du, Z.-y., Engling, G., Liu, J.-m., Ma, Y.-l., Zheng, M., and Weber, R. J.: The characteristics of brown carbon aerosol during winter in Beijing, *Atmos. Environ.*, 127, 355-364, <https://doi.org/10.1016/j.atmosenv.2015.12.035>, 2016.
- Coble, P. G.: Characterization of marine and terrestrial DOM in seawater using excitation-emission matrix spectroscopy, *Mar. Chem.*, 51, 325-346, [https://doi.org/10.1016/0304-4203\(95\)00062-3](https://doi.org/10.1016/0304-4203(95)00062-3), 1996.
- Coggon, M. M., Veres, P. R., Yuan, B., Koss, A., Warneke, C., Gilman, J. B., Lerner, B. M., Peischl, J., Aikin, K. C., Stockwell, C. E., Hatch, L. E., Ryerson, T. B., Roberts, J. M., Yokelson, R. J., and de Gouw, J. A.: Emissions of nitrogen-containing organic compounds from the burning of herbaceous and arboraceous biomass: Fuel composition dependence and the variability of commonly used nitrile tracers, *Geophys. Res. Lett.*, 43, 9903-9912, [10.1002/2016gl070562](https://doi.org/10.1002/2016gl070562), 2016.
- Cory, R. M., and Mcknight, D. M.: Fluorescence Spectroscopy Reveals Ubiquitous Presence of Oxidized and Reduced Quinones in Dissolved Organic Matter, *Environ. Sci. Technol.*, 39, 8142-8149, <https://doi.org/10.1021/es0506962>, 2005.
- Cui, M., Chen, Y., Zheng, M., Li, J., Tang, J., Han, Y., Song, D., Yan, C., Zhang, F., Tian, C., and Zhang, G.: Emissions and characteristics of particulate matter from rainforest burning in the Southeast Asia, *Atmos. Environ.*, 191, 194-204, <https://doi.org/10.1016/j.atmosenv.2018.07.062>, 2018.
- Dasari, S., Andersson, A., Bikkina, S., Holmstrand, H., Budhavant, K., Satheesh, S. K., Asmi, E., Kesti, J., Backman, J., and Salam, A.: Photochemical degradation affects the light absorption of water-soluble brown carbon in the South Asian outflow, *Science Advances*, 5, <https://doi.org/10.1126/sciadv.aau8066>, 2019.
- Di Lorenzo, R. A., Washenfelter, R. A., Attwood, A. R., Guo, H., Xu, L., Ng, N. L., Weber, R. J., Baumann, K., Edgerton, E., and Young, C. J.: Molecular-Size-Separated Brown Carbon Absorption for Biomass-Burning Aerosol at Multiple Field Sites, *Environ. Sci. Technol.*, <https://doi.org/10.1021/acs.est.6b06160>, 2017.

- Fan, X., Song, J., and Peng, P. a.: Comparison of isolation and quantification methods to measure humic-like substances (HULIS) in atmospheric particles, *Atmos. Environ.*, 60, 366-374, <https://doi.org/10.1016/j.atmosenv.2012.06.063>, 2012.
- Fan, X., Wei, S., Zhu, M., Song, J., and Peng, P. a.: Comprehensive characterization of humic-like substances in smoke PM_{2.5} emitted from the combustion of biomass materials and fossil fuels, *Atmos. Chem. Phys.*, 16, 13321-13340, <https://doi.org/10.5194/acp-16-13321-2016>, 2016.
- Feng, S., Zhang, L., Wang, S., Nadykto, A. B., Xu, Y., Shi, Q., Jiang, B., and Qian, W.: Characterization of dissolved organic nitrogen in wet deposition from Lake Erhai basin by using ultrahigh resolution FT-ICR mass spectrometry, *Chemosphere*, 156, 438-445, <https://doi.org/10.1016/j.chemosphere.2016.04.039>, 2016.
- Feng, Y., Ramanathan, V., and Kotamarthi, V. R.: Brown carbon: a significant atmospheric absorber of solar radiation?, *Atmos. Chem. Phys.*, 13, 8607-8621, <https://doi.org/10.5194/acp-13-8607-2013>, 2013.
- Fleming, L. T., Lin, P., Laskin, A., Laskin, J., Weltman, R., Edwards, R., Arora, N. K., Yadav, A., Meinardi, S., and Blake, D. R.: Molecular Composition of Particulate Matter Emissions from Dung and Brushwood Burning Household Cookstoves in Haryana, India, *Atmos. Chem. Phys.*, 18, 2461-2480, <https://doi.org/10.5194/acp-18-2461-2018>, 2017.
- Fu, P., Kawamura, K., Chen, J., Qin, M., Ren, L., Sun, Y., Wang, Z., Barrie, L. A., Tachibana, E., Ding, A., and Yamashita, Y.: Fluorescent water-soluble organic aerosols in the High Arctic atmosphere, *Sci Rep*, 5, 9845, <https://doi.org/10.1038/srep09845>, 2015.
- Gentner, D. R., Jathar, S. H., Gordon, T. D., Bahreini, R., Day, D. A., El Haddad, I., Hayes, P. L., Pieber, S. M., Platt, S. M., de Gouw, J., Goldstein, A. H., Harley, R. A., Jimenez, J. L., Prevot, A. S., and Robinson, A. L.: Review of Urban Secondary Organic Aerosol Formation from Gasoline and Diesel Motor Vehicle Emissions, *Environ. Sci. Technol.*, 51, 1074-1093, <https://doi.org/10.1021/acs.est.6b04509>, 2017.
- Ghidotti, M., Fabbri, D., Masek, O., Mackay, C. L., Montalti, M., and Hornung, A.: Source and Biological Response of Biochar Organic Compounds Released into Water; Relationships with Bio-Oil Composition and Carbonization Degree, *Environ. Sci. Technol.*, 51, 6580-6589, <https://doi.org/10.1021/acs.est.7b00520>, 2017.
- Graber, E. R., and Rudich, Y.: Atmospheric HULIS: How humic-like are they? A comprehensive and critical review, *Atmos. Chem. Phys.*, 6, 729-753, <https://doi.org/10.5194/acp-6-729-2006>, 2006.
- Gu, Q., and Kenny, J. E.: Improvement of Inner Filter Effect Correction Based on Determination of Effective Geometric Parameters Using a Conventional Fluorimeter, *Anal. Chem.*, 81, 420-426, <https://doi.org/10.1021/ac801676j>, 2009.
- Hecobian, A., Zhang, X., Zheng, M., Frank, N., Edgerton, E. S., and Weber, R. J.: Water-Soluble Organic Aerosol material and the light-absorption characteristics of aqueous extracts measured over the Southeastern United States, *Atmos. Chem. Phys.*, 10, 5965-5977,

882 <https://doi.org/10.5194/acp-10-5965-2010>, 2010.

883 Jiang, B., Kuang, B. Y., Liang, Y., Zhang, J., Huang, X. H. H., Xu, C., Yu, J. Z., and Shi, Q.:
 884 Molecular composition of urban organic aerosols on clear and hazy days in Beijing: a
 885 comparative study using FT-ICR MS, *Environ. Chem.*, 13, 888-901,
 886 <https://doi.org/10.1071/en15230>, 2016.

887 Kirchstetter, T. W., and Thatcher, T. L.: Contribution of organic carbon to wood smoke particulate
 888 matter absorption of solar radiation, *Atmos. Chem. Phys.*, 12, 5803-5816,
 889 <https://doi.org/10.5194/acp-12-6067-2012>, 2012.

890 Koch, B., and Dittmar, T.: Koch, B. P. & Dittmar, T. From mass to structure: An aromaticity
 891 index for high-resolution mass data of natural organic matter. *Rapid Commun. Mass*
 892 *Spectrom.* 20, 926-932, *Rapid Commun. Mass Spectrom.*, 20, 926-932,
 893 <https://doi.org/10.1002/rcm.2386>, 2006.

894 Kumar, N. K., Corbin, J. C., Bruns, E. A., Massabó, D., Slowik, J. G., Drinovec, L., Močnik, G.,
 895 Prati, P., Vlachou, A., Baltensperger, U., Gysel, M., El-Haddad, I., and Prévôt, A. S. H.:
 896 Production of particulate brown carbon during atmospheric aging of residential
 897 wood-burning emissions, *Atmos. Chem. Phys.*, 18, 17843-17861,
 898 <https://doi.org/10.5194/acp-18-17843-2018>, 2018.

899 Laskin, A., Laskin, J., and Nizkorodov, S. A.: Chemistry of atmospheric brown carbon, *Chem.*
 900 *Rev.*, 115, 4335-4382, <https://doi.org/10.1021/cr5006167>, 2015.

901 Laskin, A., Smith, J. S., and Laskin, J.: Molecular Characterization of Nitrogen-Containing
 902 Organic Compounds in Biomass Burning Aerosols Using High-Resolution Mass
 903 Spectrometry, *Environ. Sci Technol.*, 43, 3764-3771, <https://doi.org/10.1021/es803456n>,
 904 2009.

905 Lee, H. J., Laskin, A., Laskin, J., and Nizkorodov, S. A.: Excitation-emission spectra and
 906 fluorescence quantum yields for fresh and aged biogenic secondary organic aerosols, *Environ.*
 907 *Sci Technol.*, 47, 5763-5770, <https://doi.org/10.1021/es400644c>, 2013.

908 Li, C., He, Q., Schade, J., Passig, J., Zimmermann, R., Meidan, D., Laskin, A., and Rudich, Y.:
 909 Dynamic changes in optical and chemical properties of tar ball aerosols by atmospheric
 910 photochemical aging, *Atmos. Chem. Phys.*, 19, 139-163,
 911 <https://doi.org/10.5194/acp-19-139-2019>, 2019.

912 Li, M., Fan, X., Zhu, M., Zou, C., Song, J., Wei, S., Jia, W., and Peng, P.: Abundances and light
 913 absorption properties of brown carbon emitted from residential coal combustion in China,
 914 *Environ. Sci. Technol.*, 53, 595-603, <https://doi.org/10.1021/acs.est.8b05630>, 2018.

915 Lin, P., Rincon, A. G., Kalberer, M., and Yu, J. Z.: Elemental composition of HULIS in the Pearl
 916 River Delta Region, China: results inferred from positive and negative electrospray high
 917 resolution mass spectrometric data, *Environ. Sci. Technol.*, 46, 7454-7462,
 918 <https://doi.org/10.1021/es300285d>, 2012a.

919 Lin, P., Yu, J. Z., Engling, G., and Kalberer, M.: Organosulfates in humic-like substance fraction

isolated from aerosols at seven locations in East Asia: a study by ultra-high-resolution mass spectrometry, *Environ. Sci. Technol.*, 46, 13118-13127, <https://doi.org/10.1021/es303570v>, 2012b.

Lin, P., Aiona, P. K., Li, Y., Shiraiwa, M., Laskin, J., Nizkorodov, S. A., and Laskin, A.: Molecular Characterization of Brown Carbon in Biomass Burning Aerosol Particles, *Environ. Sci. Technol.*, 50, 11815-11824, <https://doi.org/10.1021/acs.est.6b03024>, 2016.

Lin, P., Fleming, L. T., Nizkorodov, S. A., Laskin, J., and Laskin, A.: Comprehensive Molecular Characterization of Atmospheric Brown Carbon by High Resolution Mass Spectrometry with Electrospray and Atmospheric Pressure Photoionization, *Anal. Chem.*, 90, 12493-12502, <https://doi.org/10.1021/acs.analchem.8b02177>, 2018.

Liu, J., Bergin, M., Guo, H., King, L., Kotra, N., Edgerton, E., and Weber, R. J.: Size-resolved measurements of brown carbon in water and methanol extracts and estimates of their contribution to ambient fine-particle light absorption, *Atmos. Chem. Phys.*, 13, 12389-12404, <https://doi.org/10.5194/acp-13-12389-2013>, 2013.

Liu, J., Mo, Y., Ding, P., Li, J., Shen, C., and Zhang, G.: Dual carbon isotopes ((^{14}C) and (^{13}C)) and optical properties of WSOC and HULIS-C during winter in Guangzhou, China, *Sci. Total Environ.*, 633, 1571-1578, <https://doi.org/10.1016/j.scitotenv.2018.03.293>, 2018.

Luciani, X., Mounier, S., Redon, R., and Bois, A.: A simple correction method of inner filter effects affecting FEEM and its application to the PARAFAC decomposition, *Chemom. Intell. Lab. Syst.*, 96, 227-238, <https://doi.org/10.1016/j.chemolab.2009.02.008>, 2009.

Lv, J., Zhang, S., Wang, S., Luo, L., Cao, D., and Christie, P.: Molecular-Scale Investigation with ESI-FT-ICR-MS on Fractionation of Dissolved Organic Matter Induced by Adsorption on Iron Oxyhydroxides, *Environ. Sci. Technol.*, 50, 2328-2336, <https://doi.org/10.1021/acs.est.5b04996>, 2016.

Matos, J. T. V., Freire, S. M. S. C., Duarte, R. M. B. O., and Duarte, A. C.: Natural organic matter in urban aerosols: Comparison between water and alkaline soluble components using excitation–emission matrix fluorescence spectroscopy and multiway data analysis, *Atmos. Environ.*, 102, 1-10, <https://doi.org/10.1016/j.atmosenv.2014.11.042>, 2015.

Mazzoleni, L. R., Ehrmann, B. M., Shen, X. H., Marshall, A. G., and Collett, J. L.: Water-Soluble Atmospheric Organic Matter in Fog: Exact Masses and Chemical Formula Identification by Ultrahigh-Resolution Fourier Transform Ion Cyclotron Resonance Mass Spectrometry, *Environ. Sci. Technol.*, 44, 3690-3697, <https://doi.org/10.1021/es903409k>, 2010.

Mo, Y., Li, J., Jiang, B., Su, T., Geng, X., Liu, J., Jiang, H., Shen, C., Ding, P., Zhong, G., Cheng, Z., Liao, Y., Tian, C., Chen, Y., and Zhang, G.: Sources, compositions, and optical properties of humic-like substances in Beijing during the 2014 APEC summit: Results from dual carbon isotope and Fourier-transform ion cyclotron resonance mass spectrometry analyses, *Environ. Pollut.*, 239, 322-331, <https://doi.org/10.1016/j.envpol.2018.04.041>, 2018.

Mo, Y. Z., Li, J., Liu, J. W., Zhong, G. C., Cheng, Z. N., Tian, C. G., Chen, Y. J., and Zhang, G.:

The influence of solvent and pH on determination of the light absorption properties of
 water-soluble brown carbon, *Atmos. Environ.*, 161, 90-98,
<https://doi.org/10.1016/j.atmosenv.2017.04.037>, 2017.

Murphy, K. R., Butler, K. D., Spencer, R. G., Stedmon, C. A., Boehme, J. R., and Aiken, G. R.:
 Measurement of dissolved organic matter fluorescence in aquatic environments: an
 interlaboratory comparison, *Environ. Sci. Technol.*, 44, 9405-9412,
<https://doi.org/10.1021/es102362t>, 2010.

Murphy, K. R., Stedmon, C. A., Graeber, D., and Bro, R.: Fluorescence spectroscopy and
 multi-way techniques. PARAFAC, *Anal. Methods*, 5, 6557-6566,
<https://doi.org/10.1039/c3ay41160e>, 2013.

Park, S., Yu, G.-H., and Lee, S.: Optical absorption characteristics of brown carbon aerosols
 during the KORUS-AQ campaign at an urban site, *Atmos. Res.*, 203, 16-27,
<https://doi.org/10.1016/j.atmosres.2017.12.002>, 2018.

Park, S. S., and Yu, J.: Chemical and light absorption properties of humic-like substances from
 biomass burning emissions under controlled combustion experiments, *Atmos. Environ.*, 136,
 114-122, <https://doi.org/10.1016/j.atmosenv.2016.04.022>, 2016.

Qin, J., Zhang, L., Zhou, X., Duan, J., Mu, S., Xiao, K., Hu, J., and Tan, J.: Fluorescence
 fingerprinting properties for exploring water-soluble organic compounds in PM 2.5 in an
 industrial city of northwest China, *Atmos. Environ.*, 184, 203-211,
<https://doi.org/10.1016/j.atmosenv.2018.04.049>, 2018.

Saleh, R., Robinson, E. S., Tkacik, D. S., Ahern, A. T., Liu, S., Aiken, A. C., Sullivan, R. C.,
 Presto, A. A., Dubey, M. K., Yokelson, R. J., Donahue, N. M., and Robinson, A. L.:
 Brownness of organics in aerosols from biomass burning linked to their black carbon content,
Nat. Geosci., 7, 647-650, <https://doi.org/10.1038/ngeo2220>, 2014.

Schmitt-Kopplin, P., Gelencser, A., Dabek-Zlotorzynska, E., Kiss, G., Hertkorn, N., Harir, M.,
 Hong, Y., and Gebefugi, I.: Analysis of the Unresolved Organic Fraction in Atmospheric
 Aerosols with Ultrahigh-Resolution Mass Spectrometry and Nuclear Magnetic Resonance
 Spectroscopy: Organosulfates As Photochemical Smog Constituents, *Anal. Chem.*, 82,
 8017-8026, <https://doi.org/10.1021/ac101444r>, 2010.

Sgroi, M., Roccaro, P., Korshin, G. V., and Vagliasindi, F. G. A.: Monitoring the Behavior of
 Emerging Contaminants in Wastewater-Impacted Rivers Based on the Use of Fluorescence
 Excitation Emission Matrixes (EEM), *Environ. Sci. Technol.*, 51, 4306-4316,
<https://doi.org/10.1021/acs.est.6b05785>, 2017.

Shetty, N. J., Pandey, A., Baker, S., Hao, W. M., and Chakrabarty, R. K.: Measuring light
 absorption by freshly emitted organic aerosols: optical artifacts in traditional
 solvent-extraction-based methods, *Atmos. Chem. Phys.*, 19, 8817-8830,
<https://doi.org/10.5194/acp-19-8817-2019>, 2019.

Shimabuku, K. K., Kennedy, A. M., Mulhern, R. E., and Summers, R. S.: Evaluating Activated

996 Carbon Adsorption of Dissolved Organic Matter and Micropollutants Using Fluorescence
 997 Spectroscopy, *Environ. Sci. Technol.*, 51, 2676-2684, <https://doi.org/10.1021/acs.est.6b04911>,
 998 2017.

999 Sleighter, R. L., Chen, H., Wozniak, A. S., Willoughby, A. S., Caricasole, P., and Hatcher, P. G.:
 1000 Establishing a measure of reproducibility of ultrahigh-resolution mass spectra for complex
 1001 mixtures of natural organic matter, *Anal. Chem.*, 84, 9184-9191,
 1002 <https://doi.org/10.1021/ac3018026>, 2012.

1003 Smith, J. S., Laskin, A., and Laskin, J.: Molecular Characterization of Biomass Burning Aerosols
 1004 Using High-Resolution Mass Spectrometry, *Anal. Chem.*, 81, 1512-1521, 2009.

1005 Song, J., Li, M., Jiang, B., Wei, S., Fan, X., and Peng, P.: Molecular Characterization of
 1006 Water-Soluble Humic like Substances in Smoke Particles Emitted from Combustion of
 1007 Biomass Materials and Coal Using Ultrahigh-Resolution Electrospray Ionization Fourier
 1008 Transform Ion Cyclotron Resonance Mass Spectrometry, *Environ. Sci. Technol.*, 52,
 1009 2575-2585, <https://doi.org/10.1021/acs.est.7b06126>, 2018.

1010 Song, J., Li, M., Fan, X., Zou, C., Zhu, M., Jiang, B., Yu, Z., Jia, W., Liao, Y., and Peng, P. a.:
 1011 Molecular characterization of water- and methanol-soluble organic compounds emitted from
 1012 residential coal combustion using ultrahigh-resolution electrospray ionization Fourier
 1013 transform ion cyclotron resonance mass spectrometry, *Environ. Sci. Technol.*,
 1014 <https://doi.org/10.1021/acs.est.9b04331>, 2019.

1015 Stubbins, A., Lapierre, J. F., Berggren, M., Prairie, Y. T., Dittmar, T., and del Giorgio, P. A.:
 1016 What's in an EEM? Molecular signatures associated with dissolved organic fluorescence in
 1017 boreal Canada, *Environ. Sci. Technol.*, 48, 10598-10606, <https://doi.org/10.1021/es502086e>,
 1018 2014.

1019 Sun, H., Biedermann, L., and Bond, T. C.: Color of brown carbon: A model for ultraviolet and
 1020 visible light absorption by organic carbon aerosol, *Geophys. Res. Lett.*, 34,
 1021 <https://doi.org/10.1029/2007gl029797>, 2007.

1022 Tao, S., Lu, X., Levac, N., Bateman, A. P., Nguyen, T. B., Bones, D. L., Nizkorodov, S. A.,
 1023 Laskin, J., Laskin, A., and Yang, X.: Molecular Characterization of Organosulfates in
 1024 Organic Aerosols from Shanghai and Los Angeles Urban Areas by Nanospray-Desorption
 1025 Electrospray Ionization High-Resolution Mass Spectrometry, *Environ. Sci. Technol.*, 48,
 1026 10993-11001, <https://doi.org/10.1021/es5024674>, 2014.

1027 Tian, J., Ni, H., Cao, J., Han, Y., Wang, Q., Wang, X., Chen, L. W. A., Chow, J. C., Watson, J. G.,
 1028 Wei, C., Sun, J., Zhang, T., and Huang, R.: Characteristics of carbonaceous particles from
 1029 residential coal combustion and agricultural biomass burning in China, *Atmos. Pollut. Res.*, 8,
 1030 521-527, <https://doi.org/10.1016/j.apr.2016.12.006>, 2017.

1031 Wang, Y., Hu, M., Lin, P., Guo, Q., Wu, Z., Li, M., Zeng, L., Song, Y., Zeng, L., Wu, Y., Guo, S.,
 1032 Huang, X., and He, L.: Molecular Characterization of Nitrogen-Containing Organic
 1033 Compounds in Humic-like Substances Emitted from Straw Residue Burning, *Environ. Sci.*

- Technol., 51, 5951-5961, <https://doi.org/10.1021/acs.est.7b00248>, 2017.
- Wells, M. J. M., Mullins, G. A., Bell, K. Y., Da Silva, A. K., and Navarrete, E. M.: Fluorescence and Quenching Assessment (EEM-PARAFAC) of de Facto Potable Reuse in the Neuse River, North Carolina, United States, *Environ. Sci. Technol.*, 51, 13592-13602, <https://doi.org/10.1021/acs.est.7b03766>, 2017.
- Wong, J. P. S., Nenes, A., and Weber, R. J.: Changes in Light Absorptivity of Molecular Weight Separated Brown Carbon Due to Photolytic Aging, *Environ. Sci. Technol.*, 51, 8414-8421, <https://doi.org/10.1021/acs.est.7b01739>, 2017.
- Wozniak, A. S., Bauer, J. E., Sleighter, R. L., Dickhut, R. M., and Hatcher, P. G.: Technical Note: Molecular characterization of aerosol-derived water soluble organic carbon using ultrahigh resolution electrospray ionization Fourier transform ion cyclotron resonance mass spectrometry, *Atmos. Chem. Phys.*, 8, 5099-5111, <https://doi.org/10.5194/acp-8-5099-2008>, 2008.
- Wu, G., Ram, K., Fu, P., Wang, W., Zhang, Y., Liu, X., Stone, E. A., Pradhan, B. B., Dangol, P. M., Panday, A. K., Wan, X., Bai, Z., Kang, S., Zhang, Q., and Cong, Z.: Water-Soluble Brown Carbon in Atmospheric Aerosols from Godavari (Nepal), a Regional Representative of South Asia, *Environ. Sci. Technol.*, 53, 3471-3479, <https://doi.org/10.1021/acs.est.9b00596>, 2019.
- Xie, M., Hays, M. D., and Holder, A. L.: Light-absorbing organic carbon from prescribed and laboratory biomass burning and gasoline vehicle emissions, *Sci Rep*, 7, 7318, <https://doi.org/10.1038/s41598-017-06981-8>, 2017.
- Xie, M., Chen, X., Holder, A. L., Hays, M. D., Lewandowski, M., Offenberg, J. H., Kleindienst, T. E., Jaoui, M., and Hannigan, M. P.: Light absorption of organic carbon and its sources at a southeastern U.S. location in summer, *Environ. Pollut.*, 244, 38-46, <https://doi.org/10.1016/j.envpol.2018.09.125>, 2019.
- Yan, C., Zheng, M., Sullivan, A. P., Bosch, C., Desyaterik, Y., Andersson, A., Li, X., Guo, X., Zhou, T., Gustafsson, Ö., and Collett, J. L.: Chemical characteristics and light-absorbing property of water-soluble organic carbon in Beijing: Biomass burning contributions, *Atmos. Environ.*, 121, 4-12, <https://doi.org/10.1016/j.atmosenv.2015.05.005>, 2015.
- Yan, G., and Kim, G.: Speciation and Sources of Brown Carbon in Precipitation at Seoul, Korea: Insights from Excitation-Emission Matrix Spectroscopy and Carbon Isotopic Analysis, *Environ. Sci. Technol.*, <https://doi.org/10.1021/acs.est.7b02892>, 2017.
- Yassine, M. M., Dabek-Zlotorzynska, E., Harir, M., and Schmitt-Kopplin, P.: Identification of weak and strong organic acids in atmospheric aerosols by capillary electrophoresis/mass spectrometry and ultra-high-resolution Fourier transform ion cyclotron resonance mass spectrometry, *Anal. Chem.*, 84, 6586-6594, <https://doi.org/10.1021/ac300798g>, 2012.
- Yu, H., Liang, H., Qu, F., Han, Z. S., Shao, S., Chang, H., and Li, G.: Impact of dataset diversity on accuracy and sensitivity of parallel factor analysis model of dissolved organic matter

fluorescence excitation-emission matrix, *Sci Rep*, 5, 10207,
<https://doi.org/10.1038/srep10207>, 2015.

Zhang, X., Lin, Y. H., Surratt, J. D., Zotter, P., Prevot, A. S. H., and Weber, R. J.: Light -
 absorbing soluble organic aerosol in Los Angeles and Atlanta: A contrast in secondary
 organic aerosol, *Geophys. Res. Lett.*, 38, <https://doi.org/10.1029/2011GL049385>, 2011.

Zhang, X., Lin, Y. H., Surratt, J. D., and Weber, R. J.: Sources, composition and absorption
 Angstrom exponent of light-absorbing organic components in aerosol extracts from the Los
 Angeles Basin, *Environ. Sci. Technol.*, 47, 3685-3693, <https://doi.org/10.1021/es305047b>,
 2013.

Zhang, Y., Yuan, Q., Huang, D., Kong, S., Zhang, J., Wang, X., Lu, C., Shi, Z., Zhang, X., Sun,
 Y., Wang, Z., Shao, L., Zhu, J., and Li, W.: Direct Observations of Fine Primary Particles
 From Residential Coal Burning: Insights Into Their Morphology, Composition, and
 Hygroscopicity, *Journal of Geophysical Research: Atmospheres*, 123, 12,964-912,979,
<https://doi.org/10.1029/2018jd028988>, 2018.

Zhao, Y., Hallar, A. G., and Mazzoleni, L. R.: Atmospheric organic matter in clouds: exact masses
 and molecular formula identification using ultrahigh-resolution FT-ICR mass spectrometry,
Atmos. Chem. Phys., 13, 12343-12362, <https://doi.org/10.5194/acp-13-12343-2013>, 2013.

Zhu, C. S., Cao, J. J., Huang, R. J., Shen, Z. X., Wang, Q. Y., and Zhang, N. N.: Light absorption
 properties of brown carbon over the southeastern Tibetan Plateau, *Sci. Total Environ.*, 625,
 246-251, <https://doi.org/10.1016/j.scitotenv.2017.12.183>, 2018.